Carnets Geol. 17 (3)

E-ISSN 1634-0744
DOI 10.4267/2042/62267

Sedimentological investigation on Holocene deposits in the Mussafah channel (Abu Dhabi, United Arab Emirates)

Bruno GRANIER [1]

Robert BOICHARD [2]

Abstract: Eight macrofacies types (5) plus subtypes (3) were identified while measuring sections along the Mussafah channel profile. These include:
• aeolian sands,
• microbial mat and microbial-laminated sediments,
• gypsum and enterolithic anhydrite, *i.e.*, a diagenetic variation of the previous facies,
• muds with small pelecypods, and • its seagrass meadow version,
• Potamid sands, and • its cemented version, *i.e.*, the Potamid beach-rock,
• washover fan coquina.

A complete set of analyses, including granulometry, mineral composition, clay composition, TOC, and identification of the allochems and the microfossils, was performed on this material. The facies and their genetic setting, *i.e.*, the sequence of facies, provide a perspective on both the environmental and stratigraphical significance of their distribution, both lateral and vertical, and an example of the application of the WALTHER's law. The lower microbial mat is the mark of a transgression whereas the upper microbial mat is the mark of a forced regression. In conclusion, the sequence of facies allows identification of the last Holocene transgressive-regressive cycle that includes a forced regression, which probably dates back to 6,000 years BP.

Key-words:

• Holocene;
• Flandrian;
• Abu Dhabi;
• Persian Gulf;
• facies;
• transgression;
• forced regression

Citation: GRANIER B. & BOICHARD R. (2017).- Sedimentological investigation on Holocene deposits in the Mussafah channel (Abu Dhabi, United Arab Emirates).- *Carnets Geol.*, Madrid, vol. 17, no. 3, p. 39-104.

Résumé : ***Recherches sédimentologiques sur des dépôts holocènes dans le canal de Mussafah (Abou Dabi, Émirats Arabes Unis).-*** Huit macrofaciès (5 types et 3 sous-types) ont été reconnus au cours de levés de coupes sériées le long du canal de Mussafah et dans son prolongement. Il s'agit :
• de sables éoliens,
• du tapis microbien et des sédiments à laminations microbiennes associés,
• de gypse et d'anhydrite entérolithique, soit une variante diagénétique du faciès précédent,
• de boues à petits bivalves et • de sa version d'herbier marin,
• de sables à Potamides et • de leur version cimentée, soit le grès de plage à Potamides,
• de lumachelles de dépôts de débordement.

Un ensemble complet d'analyses, comprenant granulométrie, composition minéralogique, fraction argileuse, COT, identification des microfossiles et autres éléments figurés, a été réalisé sur ce matériel. Les faciès et leur cadre génétique, c'est-à-dire la séquence de faciès, donnent une idée de l'importance à la fois environnementale et stratigraphique de leur répartition, à la fois latéralement et verticalement, et

[1] *Dépt. STU, Fac. Sci. Tech., UBO, 6 avenue Le Gorgeu, CS 93837, F-29238 Brest (France)*
bgranier@univ-brest.fr
Department of Ecology and Evolutionary Biology, The University of Kansas, 1200 Sunnyside Avenue, Lawrence, Kansas 66045 (USA)
bgranier@ku.edu
[2] *TOTAL E&P, Geo-Technology Solutions, Office BA2019, TOTAL - CSTJF, avenue Larribau, 64018 Pau (France)*
robert.boichard@total.com

Published online in final form (pdf) on June 25, 2017
[Editor: Michel MOULLADE; language editor: Phil SALVADOR; technical editor: Bruno GRANIER]

fournissent un exemple d'utilisation de la loi de WALTHER. Le tapis microbien inférieur est la marque d'une transgression alors que le tapis microbien supérieur apparaît comme celle d'une régression forcée. En conclusion, la séquence de faciès permet d'identifier le dernier cycle transgressif-régressif holocène qui comprend une régression forcée débutant probablement vers 6000 ans avant J.C.

Mots-clefs :

- Holocène ;
- Flandrien ;
- Abou Dabi ;
- Golfe persique ;
- faciès ;
- transgression ;
- régression forcée

1. Introduction

The Mussafah channel is located on the south-eastern side of Khor Qirqishan, the lagoon bordering the Abu Dhabi city island on its south-western side (Fig. 1). This entirely artificial structure was cut inland in 1985 over a distance of some six kilometers almost perpendicular to the coastline, *i.e.*, in a roughly East-West direction.

The Mussafah channel transect (Poster 1) has been reconstructed from partial sections distributed over a total length of some seven kilometers along the channel or on its axial projection. These sections were examined in 1986 and 1987. They are two hundred meters apart on average and are identified on the basis of their distance from the beginning of the transect along the channel (Poster 1).

Figure 1: A) Location (satellite image) of the Mussafah channel, Abu Dhabi (Images © 2016 TerraMetrics, Données cartographiques © Google). **B)** Enlargement of the orange rectangle with the red dotted contour of the channel in 1987 and its blue full contour in 2016.

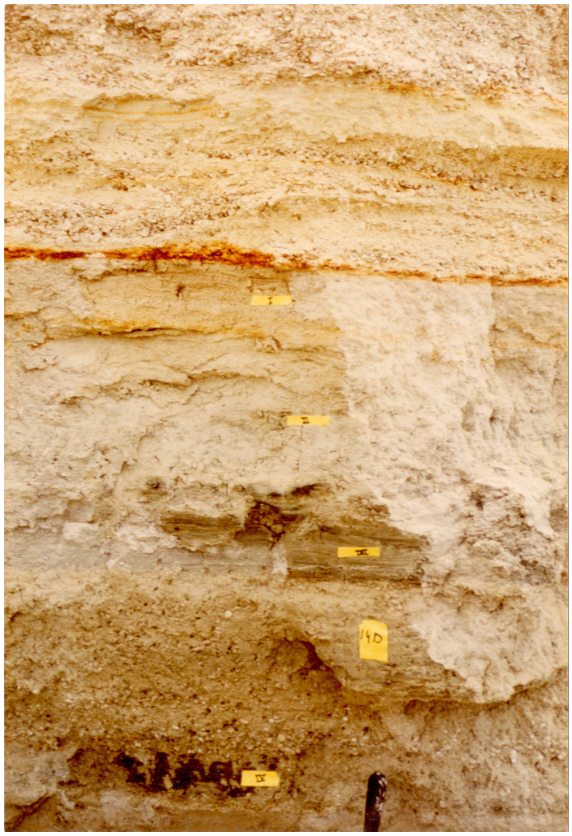

Figure 2: Site 14 D.

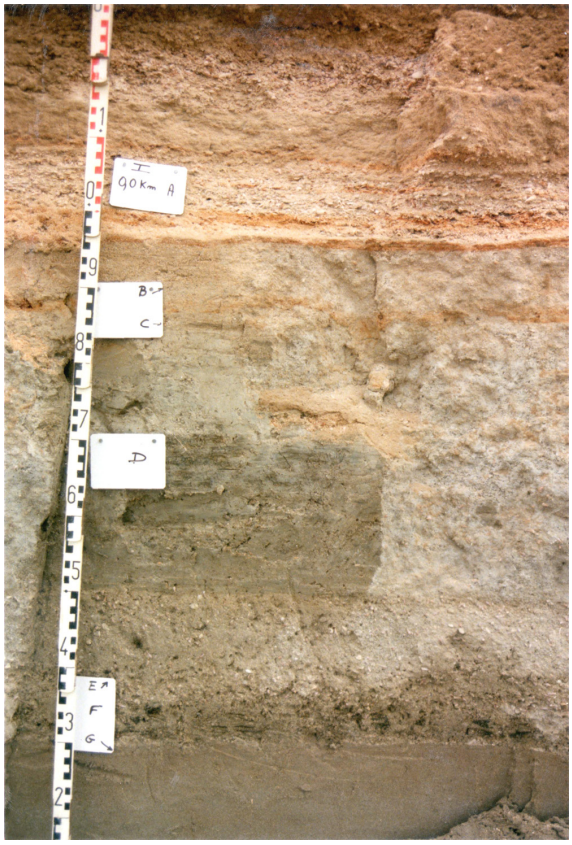

Figure 3: 0 km mark.

A

B

Figure 4: A) Site 14 B; **B)** Detail of the lower microbial mat at site 14 B.

A preliminary (unpublished) TOTAL internal report was issued the next year (Granier, 1988) followed by Kenig's PhD thesis (1991) and a set of works that focus on the distribution of organic matter in the Holocene sediments of Abu Dhabi (Kenig *et al.*, 1990; Baltzer *et al.*, 1994; Kenig, 2011). Six of the studied sections were examined in greater detail, involving sediment sampling. They correspond to -2 km, 0 km, 0.6 km, 1.6 km, 4.2 km, and 6 km marks. Field information gathered in this study is supplemented by data from two additional sections (sites 14 B and 14 D), visited in an earlier excursion in 1986, and from a trench dug two kilometers downdip of the western end of the channel. The studied sections are:

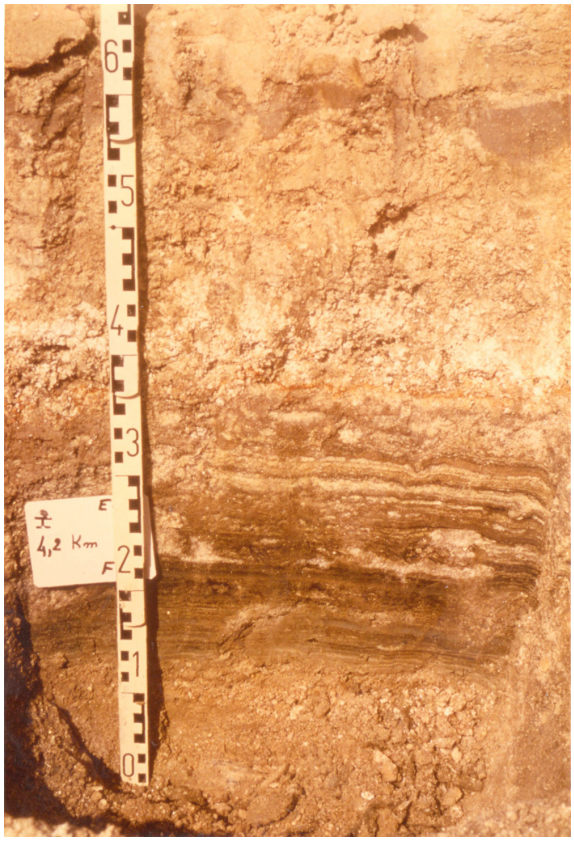

Figure 5: 4.2 km mark.

Figure 6: 6 km mark.

- -2 km mark (Poster 2),
- site 14 D (Fig. 2 ; Poster 3),
- 0 km mark (Fig. 3 ; Poster 4),
- site 14 B (Fig. 4 ; Poster 5),
- 0.6 km mark (Poster 6),
- 1.6 km mark (Poster 7),
- 4.2 km mark (Fig. 5 ; Poster 8),
- 6 km mark (Fig. 6 ; Poster 9).

Most depositional facies observed along the Holocene Mussafah channel transect are currently observed on the coastal margins of the inner lagoonal areas of Abu Dhabi island where they are roughtly arranged in "living" facies belts, as recorded in the literature (*e.g.*, KENDALL & SKIPWITH, 1969a, 1969b; EVANS *et al.*, 1973; ALSHARHAN & KENDALL, 2003). The few remaining facies correspond to the fossil or diagenetic counterparts of modern facies. Using an approach similar to that of WAGNER and van der TOGT (1973), a complete set of simple analyses (including microfacies analyses) was then run to help identifying the primary depositional macrofacies. The reconstruction of the horizontal and vertical sequence of facies enabled us to partly unravel of the last Holocene sedimentary cycle in the area studied.

2. Material and methods

More than sixty **unconsolidated samples** were weighed before wet sieving and splitting into four grain size categories:

- grains between 0.063 and 0.125 mm: silts,
- grains between 0.125 and 0.250 mm: fine sands,
- grains between 0.250 and 2 mm: medium to very coarse sands,
- grains larger than 2 mm: pebbles.

For each sample all of these categories were dried, then weighted. The results are expressed as a percentage of the original dry weight of the sample (Table 1; Poster 10). The value for a fifth category that groups all those particles finer than 63 µm, *e.g.*, lime mud, clay minerals, organic matter, or sulphate salts, was back-calculated from the difference between the above summation and the original dry weight.

Finally, discrete allochem types ranging in size from 0.250 to 2 mm were identified using stereoscopic lenses and their proportion of the total population expressed as a percentage (Table 2). By comparison, WAGNER and van der TOGT (1973) were only considering three categories (finer than 63 µm, between 63 µm and 2 mm, larger than 2 mm).

Table 1: Grain sizes (%).

Stops	Sample no.	> 2,000 µm	250-2,000 µm	125-250 µm	63-125 µm
14B-I	ABA 93	0.0	4.9	19.3	19.6
14B-II	ABA 94	0.3	3.1	5.7	22.6
14B-III	ABA 95	2.5	2.5	5.6	19.3
14B-IV	ABA 96	0.0	12.9	52.9	29.4
14B-V	ABA 97	0.0	1.7	24.3	59.0
14B-VI	ABA 98	41.7	28.9	9.4	2.4
14D-I	ABA 99	2.7	24.1	10.8	12.7
14D-II	ABA 100	0.3	1.2	2.0	11.1
14D-III	ABA 101	0.0	2.6	12.3	29.2
14D-IIIDis	ABA 102	17.5	25.6	25.1	18.3
14D-IV	ABA 103	0.8	11.5	18.6	20.5
14D-V	ABA 104	0.0	15.3	55.3	22.3
14E-I	ABA 105	0.0	0.1	0.1	2.4
14E-II	ABA 106	0.0	0.0	0.1	0.9
14E-III	ABA 107	0.0	0.6	0.7	5.7
14E-	ABA 110	0.7	1.8	2.5	6.0
0 km-A	ABA 121	28.6	53.9	9.3	3.4
0.2 km-A	ABA 122	25.7	13.3	18.1	5.3
0.6 km-A	ABA 123	0.1	1.8	23.8	37.1
1.6 km-A	ABA 124	0.0	2.6	4.8	17.3
4.2 km-A	ABA 126	0.0	0.3	4.5	29.8
0.2 km-A1	ABA 127	7.3	75.2	12.2	2.3
0.2 km-A2	ABA 128	94.2	1.7	1.0	0.9
-2 km-A	ABA 129	12.0	9.6	2.7	6.6
0 km-B	ABA 131	0.4	18.1	9.6	14.7
0.6 km-B	ABA 132	0.1	4.0	16.9	18.7
1.6 km-B	ABA 133	2.6	15.8	3.8	11.6
4.2 km-B	ABA 134	0.0	0.1	0.9	15.8
6.0 km-B	ABA 135	0.0	2.2	5.0	19.3
-2 km-B	ABA 136	0.0	3.9	1.2	6.9
0 km-C	ABA 137	0.0	2.3	3.1	11.5
0.6 km-C	ABA 139	0.0	4.4	19.9	24.7
1.6 km-C	ABA 140	0.3	0.1	0.2	4.6
4.2 km-C	ABA 141	0.0	0.0	0.5	9.1
6.0 km-C	ABA 142	0.0	2.3	5.7	22.7
-2 km-C	ABA 143	0.6	4.7	1.3	3.4
0 km-D	ABA 144	1.3	5.2	6.0	14.1
1.6 km-D	ABA 146	0.2	2.1	11.5	20.2
4.2 km-D	ABA 147	0.0	0.0	1.5	6.8
6.0 km-D	ABA 148	0.0	0.8	0.4	6.6
-2 km-D	ABA 149	0.0	2.7	4.6	22.1
0 km-E	ABA 150	8.0	22.4	21.5	29.0
1.6 km-E	ABA 161	10.9	29.5	14.7	17.8
4.2 km-E	ABA 162	0.0	0.0	0.3	1.6
6.0 km-E	ABA 163	0.2	6.9	1.1	3.4
-2 km-E	ABA 164	0.0	10.1	12.9	35.2
0 km-F	ABA 165	6.8	26.5	12.3	18.9
0.6 km-F	ABA 166	0.0	31.8	41.0	19.7
4.2 km-F	ABA 168	0.4	1.6	6.3	19.5
6.0 km-F	ABA 169	1.2	14.1	20.6	33.0
0 km-G	ABA 170	0.0	15.6	44.9	20.9
4.2 km-G	ABA 171	62.2	12.2	10.5	8.2
4.2 km-H	ABA 173	8.5	31.8	27.0	20.5
6.0 km-H	ABA 173bis	3.3	11.1	10.9	46.4
4.2 km-K	ABA 176	7.5	19.7	20.3	28.1
4.2 km-L	ABA 177	0.2	2.2	3.8	23.9

Table 2: Components (250 -2,000 µm).

Stops	Sample no.	sponge spicules	Echinoid spines	Decapods	Bryozoans	*Acetabularia* sp.	*Spirorbis* sp.	Pelecypods	Gastropods	Ostracods	• with smooth valves	• with longitudinal ridges or reticulate ornaments	• with an accuminate posterior margin	Foraminifers	• Miliolids	• *Miliammina fusca*	• *P. planatus* & *M. acicularis*	• *Sorites orbiculus*	• *Ammonia convexa*	• *Elphidium striatopunctatum*	• Textulariid	• Lenticulina sp.	Coralline algae	ooids	lumps, ...	"rounded grains"	faecal pellets	thin section
14B-I	ABA 93				-	-	1	-	-	-	-			1			-		1	-					91	6		
14B-II	ABA 94				-	2	1	2	1	7	7			8			6	-	2	-					72	7		
14B-III	ABA 95				-	-	-	3	2	17	17			6	-	-	4		2						68	1		
14B-IV	ABA 96		X					X						X	X						X	X	X	X		100		□
14B-V	ABA 97		X					X						X	X		X				X	X	X	X		100		□
14B-VI	ABA 98				3	10	8	21	6	-	-			14	1		11	-	1	-					38	1		□
14D-I	ABA 99					-	-	-	-					-			-								100			
14D-II	ABA 100					4	2		1	-	-			1		-	-		-						76	13	-	
14D-III	ABA 101					2	-	3	-	2	2			2			2		-						80	11		
14D-IIIDis	ABA 102				-	8	2	3	2	17	17			2			2		-						66			
14D-IV	ABA 103				-	6	4	3	3	2	2			2			2								80			
14D-V	ABA 104		X			*	*	*	-	-	-			*	X		*				X	X	X	X		100		□
0 km-A	ABA 121				-	11	6	19	8	-	-	-	-	12	2		9		1						43			
0.6 km-A	ABA 123							26	3	8	6	1	1	30	1	-	5		20	3					17	14	14	
1.6 km-A	ABA 124		*				-	X						*	X							X	X	X		100		□
4.2 km-A	ABA 126		X											X	X		X			X	X	X				100		□
-2 km-A	ABA 129																								100			□
0 km-B	ABA 131				-	1	1	2	2					1	-		-		-	-					93			
0.6 km-B	ABA 132						-	39	-	1	1	-	-	23	-	-	-		19	4					32	5	5	
1.6 km-B	ABA 133				-	-	-	-		-	-			-			-	-	-						100	-		
4.2 km-B	ABA 134		X						x					X			X			X	X		X			100		□
6.0 km-B	ABA 135				-		4	3	3	10	8	1	1	18	-		17		-						62			
-2 km-B	ABA 136																								100			□
0 km-C	ABA 137					1	1	7	1	-	-			2					2						86	2		
0.6 km-C	ABA 139							7	-	2	2	-	-	15	-	-			13	2					74	2	2	
6.0 km-C	ABA 142			-			3	6	2	3	3	-		14	1	-	11		2						54		18	
-2 km-C	ABA 143							X	X																100			□
0 km-D	ABA 144					-	3			-	-			-			-								96			
0.6 km-D	ABA 145		X		X		X	X	X	X	X			X	X		X		X				X					□
1.6 km-D	ABA 146							-		3	-	1	1	52	1	-	-		45	4						22	23	
4.2 km-D	ABA 147		X						X														X					□
6.0 km-D	ABA 148		X		X		-	*	*	-	-			*	X		-					X	X	X		100		□
-2 km-D	ABA 149		X					X	X					X	X						X	X	X	X		100		□

Stops	Sample no.	sponge spicules	Echinoid spines	Decapods	Bryozoans	*Acetabularia* sp.	*Spirorbis* sp.	Pelecypods	Gastropods	Ostracods	• with smooth valves	• with longitudinal ridges or reticulate ornaments	• with an accuminate posterior margin	Foraminifers	• Miliolids	• *Miliammina fusca*	• *P. planatus* & *M. acicularis*	• *Sorites orbiculus*	• *Ammonia convexa*	• *Elphidium striatopunctatum*	• Textulariid	• Lenticulina sp.	Coralline algae	ooids	lumps, ...	"rounded grains"	faecal pellets	thin section
0 km-E	ABA 150					3	2	1	2	15	15			4	-		1		3						73			
0.6 km-E	ABA 160							3	3	3	3	-		6	-				5	-					77	8		
1.6 km-E	ABA 161				-	6	2	11	1	-	-	-	-	16	2	-	10		4	-					60		3	
6.0 km-E	ABA 163		X		X		2	10	6	-	-			2	-		*			2		X	X			80		□
-2 km-E	ABA 164		X					X	X					X	X		X	X				X	X	X		100		
0 km-F	ABA 165		-	-	-	10	4	-	1	8	8			4	-		2		2						64	8		
0.6 km-F	ABA 166		X					X						X			X				X	X		X		100		□
1.6 km-F	ABA 167						X	X	X	X	X			X	X		X		X	X	X		X					□
4.2 km-F	ABA 168				-	-	-	3	-	-	-			2			1		-						90			
6.0 km-F	ABA 169				-	1	6	7	2	-	-			21	2	-	17	-	2	-					42		21	
0 km-G	ABA 170		*		*	1	-	*	*	3	3			-			*				X	X	X		-	96		□
4.2 km-G	ABA 171					*	-	2	1	3	3			4	*		3		1	*					88			□
6.0 km-I	ABA 172					X	X	X	X	X	X			X	X		X		X	X								□
4.2 km-H	ABA 173				-	1		2	-	1	1			8	-	-	6		-	1					87		-	
6.0 km-H	ABA 173bis	-					6	35	5	3	3	-		28	8	-	15		1	3					19		4	
4.2 km-I	ABA 174						X	X	X	X	X			X	X		X		X	X								□
4.2 km-J	ABA 175					X	X	X	X	X	X			X	X		X		X	X								□
4.2 km-K	ABA 176				-		-	11	-	-	-	-		16	6	-	4		3	3					49		21	
4.2 km-L	ABA 177				-		1	5	2	3	3			75	20	-	45		8	1					14		-	

Lithified samples and those allochems first called "rounded grains", which were barely identifiable, may require petrographic thin sections for reliable identification. In such cases only occurrences, not percentages, are reported.

Additionally, G. JOUSSON analysed the mineralogical composition of the samples by X-ray diffractometers (Table 3). Identification of the clay minerals was performed on about ten samples only (Table 4). In addition, F. KENIG analysed the Total Organic Carbon (TOC) of about fifteen samples (Table 5).

All the results of these analyses are compiled in a set of tables (Tables 2-5).

3. The allochems (larger than 0.250 mm)

Fourteen Four basic types of grains were identified: bioclasts, faecal pellets, lumps and intraclasts, and undetermined grains.

In this classification, the **bioclasts** comprise all skeletal remains the origin of which can still be clearly identified.

In this material we identified some **faecal pellets** with a peculiar spiral structure (Pl. 8, fig. 5.a-d). According to TRICHET (1967), "cette figure d'hélice serait due à une activité digestive préférentielle dans des zones de pression accentuée déterminées par la forme de l'intestin de l'animal"

Table 3: Mineralogical composition (%).

Stops	Sample no.	Mg Calcite	Aragonite	Calcite	Dolomite	Halite	Gypsum	Anhydrite	K-Feldspar	Plagioclase	Anhydrite
14B-I	ABA 93	0	27	6	5	26	0	0	0	0	6
14B-II	ABA 94	3	22	14	0	19	0	0	0	2	7
14B-III	ABA 95	4	20	14	9	18	0	0	0	4	7
14B-IV	ABA 96	0	15	46	0	3	0	0	0	5	12
14B-V	ABA 97	0	0	53	4	10	0	0	0	6	10
14B-VI	ABA 98	0	55	0	0	2	22	0	0	0	2
14D-I	ABA 99	4	39	6	5	15	0	0	0	0	3
14D-II	ABA 100	0	20	10	12	14	0	0	0	1	5
14D-III	ABA 101	4	30	9	3	29	0	0	0	0	3
14D-IIIDis	ABA 102	3	51	11	0.1	5	0	0	0	0	4
14D-IV	ABA 103	2	31	7	3	25	0	0	0	4	6
14D-V	ABA 104	0	24	46	0	5	0	0	0	0	12
0 km-A	ABA 121	3	69	9	0	3	0	0	0	0	0.1
0.2 km-A	ABA 122	3	40	11	0	12	24	0	0	0	1
0.6 km-A	ABA 123	4	33	10	8	13	0	0	0	0	4
1.6 km-A	ABA 124	0	0	14	4	13	0	35	0	3	3
3 km-A	ABA 125	0	0	5	0	4	80	0	0	0	0
4.2 km-A	ABA 126	0	0	14	31	12	0	0	4	3	7
0.2 km-A1	ABA 127	0	58	8	0	1	0	0	0	2	2
0.2 km-A2	ABA 128	0	70	5	0	1	0	0	0	0	2
-2 km-A	ABA 129	0	0	5	33	14	0	0	3	2	3
-2 km-AM	ABA 130	0	0	11	0	3	55	0	0	2	4
0 km-B	ABA 131	5	31	7	7	15	0	0	0	0	2
0.6 km-B	ABA 132	5	26	9	22	9	0	0	0	0	3
1.6 km-B	ABA 133	0	36	11	5	14	0	0	0	3	2
4.2 km-B	ABA 134	0	0	20	5	9	0	0	3	5	8
6.0 km-B	ABA 135	4	51	12	3	6	0	0	0	0	2
-2 km-B	ABA 136	0	14	4	10	10	45	0	0	2	2
0 km-C	ABA 137	3	16	9	14	16	0	0	0	3	4
0.2 km-C	ABA 138	0	20	42	0	1	0	0	0	4	9
0.6 km-C	ABA 139	4	33	6	14	8	8	0	0	0	3
1.6 km-C	ABA 140	0	0	5	8	5	45	0.1	0	0	0.1
4.2 km-C	ABA 141	0	0	10	0	5	44	9	0	0	1
6.0 km-C	ABA 142	0	0	5	0	5	59	4	0	0	0
-2 km-C	ABA 143	0	0	6	0	6	55	8	0	0	0
0 km-D	ABA 144	5	25	11	4	18	0	0	0	0	3
0.6 km-D	ABA 145	0.1	46	7	9	5	0	0	0	0	3
1.6 km-D	ABA 146	4	27	9	22	8	0	0	0	0	2
4.2 km-D	ABA 147	0	0	7	0	5	29	25	0.1	0.1	1
6.0 km-D	ABA 148	0	0	10	0	5	55	3	0	0	0
-2 km-D	ABA 149	0	0	17	3	8	0	70	0	0	1
0 km-E	ABA 150	3	47	14	0	4	0	3	0	0	7
0.6 km-E	ABA 160	0	10	17	15	20	0	0	0	0	4
1.6 km-E	ABA 161	6	43	6	19	3	0	0	0	0	3
4.2 km-E	ABA 162	0	0	5	0	5	55	0.1	0	0	0
6.0 km-E	ABA 163	0	12	8	0	4	53	0	0	0	0
-2 km-E	ABA 164	0	0	39	6	6	0	7	0	3	8
0 km-F	ABA 165	2	36	11	4	12	0	0	0	0	5
0.6 km-F	ABA 166	0	18	45	5	2	0	0	0	5	10
1.6 km-F	ABA 167	7	50	10	5	0.1	0	0	0	3	4
4.2 km-F	ABA 168	4	43	15	3	8	0	0	0	0	3
6.0 km-F	ABA 169	4	56	7	0	3	10	0	0	0	2

Stops	Sample no.	Mg Calcite	Aragonite	Calcite	Dolomite	Halite	Gypsum	Anhydrite	K-Feldspar	Plagioclase	Anhydrite
0 km-G	ABA 170	0	22	42	2	4	0	0	0	5	15
4.2 km-G	ABA 171	0	67	9	2	3	0	0	0	0	3
6.0 km-G	ABA 172	0.1	57	6	3	1	0	0	0	0	2
4.2 km-H	ABA 173	5	62	7	0	2	0	0	0	0	3
6.0 km-H	ABA 173bis	5	55	8	4	1	0	0	0	0	2
4.2 km-I	ABA 174	0	60	7	0	2	0	0	0	0	3
4.2 km-J	ABA 175	3	65	6	2	0	0	0	0	0	2
4.2 km-K	ABA 176	5	48	7	15	2	0	0	0	0	0.1
4.2 km-L	ABA 177	11	37	15	8	4	0	0	0	1	3

[this spiral shape may be related to the preferential digestive activity of the animal in zones of increased pressure determined by the morphology of its intestine]. In the same publication, the author provides information on their mineralization, *i.e.*, on the precipitation of aragonite needles within an organic matrix. In this material dolomite rhombs grew in the needle mesh and eventually replaced the aragonite (Pl. 8, fig. 6).

Lumps are aggregates of grains of various types (Pl. 15, fig. 5).

Intraclasts are by-products of *in situ* early lithification with a limited reworking.

"Rounded grains" are calcitic grains commonly eroded and centripetally micritized. A petrographic thin section may be useful to analyse such grains. In most cases they are small lithoclasts. We can thus identify inside them smaller allochems with calcitic cements (Pl. 9, figs. 1-4) and/or micritic matrices. Because all the components of these lithoclasts are truncated at their edges we assume that they probably result from the dismantling of layers already lithified and that they fall under the type defined as **extraclasts**. Constituent grains are commonly benthic foraminifers (*e.g.*, Textulariidae: Pl. 9, figs. 1 & 3-4; Lenticulinidae: Pl. 9, figs. 5-6). Thin sections made on these initially undetermined grains (17 thin sections) and on lithified samples (10 thin sections) also revealed the occurrence of **ooids**, either allochthonous (reworked from Pleistocene or older rocks), calcitic with micritic-microsparitic cortices (Pl. 10, figs. 1-2, 4-5 & 7), or autochthonous, aragonitic with micritic cortices (Pl. 11, figs. 4-5). Both types are quite different from the honey-colored ooids found in the Abu Dhabi beaches (Pl. 10, fig. 3). The mineralogical nature of these ooids was identified on thin sections coloured with a FEIGL's solution that results in a selective colouring of the aragonite.

The largest morphological and mineralogical diversity is obviously found within the **bioclasts** with macrofaunal (*e.g.*, pelecypods, gastropods, echinoderms, and sponges), microfaunal (foraminifers, ostracodes, and *Spirorbis*) and phycological remains (Rhodophyta and Chlorophyta, *e.g.*, *Acetabularia*).

Representatives of more than ten genera of **foraminifers** were identified (identifications are based on MURRAY, 1966, 1970, and HOTTINGER *et al.*, 1993) but some forms are clearly older, reworked material as, for instance, large hyaline tests referred to as *Lenticulina* (Pl. 9, figs. 5-6) and agglutined tests referred to as Textulariidae (Pl. 9, figs. 1 & 3-4), both found in extraclasts. The autochthonous forms comprise porcelaneous tests:

- either large-sized as *Peneroplis planatus* (FICHTEL & MOLL, 1798) (Pl. 6, figs. 4 *pars*, 5 & 8; Pl. 8, figs. 3-4; Pl. 9, fig. 1), which is very common,
- as well as *Monalysidium acicularis* (BATSCH, 1791) (Pl. 6, fig. 4 *pars*) and *Sorites orbiculus* (FORSKAL, 1775) (Pl. 8, figs. 1-2), which are rare,
- or small-sized miliolids as *Quinqueloculina* sp. (morphological type B of MURRAY, 1966: Pl. 5, figs. 1, 6-7 & 9; morphological type F of MURRAY, 1966: Pl. 5, figs. 10-11), *Triloculina* sp., *Spiroloculina angulata* CUSHMAN, 1917 (Pl. 5, figs. 8 & 12), which are common.

They also comprise:

- two small-sized hyalin tests: *Ammonia convexa* (COLLINS, 1958) (Pl. 5, figs. 10-14), which is very common,
- a partly agglutined test with *Miliammina fusca* (BRADY, 1870), a form that was collected in the "Muds with small pelecypod shells" (Pl. 5, figs. 2 & 5),
- and *Elphidium striatopunctatum* (FICHTEL & MOLL, 1798) (Pl. 5, figs. 7-9), which is common, and some encrusting forms referred to the Acervulinidae.

Table 4: Clay minerals (%).

Stops	Sample no.	kaolinite	illite	attapulgite	montmorillonite	chlorite
14B-V	ABA 97	14	0	40	41	5
0.6 km-B	ABA 132	9	27	33	21	10
6.0 km-B	ABA 135	13	35	39	0	13
1.6 km-C	ABA 140	11	26	30	22	11
6.0 km-C	ABA 142	12	35	41	0	12
1.6 km-D	ABA 146	28	29	20	0	23
1.6 km-E	ABA 161	26	37	17	0	20
4.2 km-F	ABA 168	20	33	31	0	16
0 km-G	ABA 170	99	0	0	0	0
4.2 km-H	ABA 173	16	31	38	0	15
4.2 km-K	ABA 176	20	29	19	17	15
4.2 km-L	ABA 177	17	34	31	0	18

Table 5: Total organic carbon (%).

Stops	Sample no.	TOC
6.0 km-A		1.80
6.0 km-B	ABA 135	1.00
6.0 km-C	ABA 142	0.45
4.2 km-E1	ABA 162-1	0.35
4.2 km-E2	ABA 162-2	0.99
4.2 km-K	ABA 176	0.24
3.6 km-A		1.57
3.0 km-A		0.00
2.6 km-A		1.00
2.6 km-B		0.58
1.6 km-B	ABA 133	0.36
1.6 km-C	ABA 140	0.22
1.6 km-D	ABA 146	0.18
1.6 km-E	ABA 161	0.18
0.6 km-E	ABA 160	1.22
0.2 km-B		0.00
0 km-B	ABA 131	0.62
0 km-C	ABA 137	0.36
0 km-D	ABA 144	0.98
0 km-F	ABA 165	1.19
-2 km-A	ABA 129	1.88
-2 km-B	ABA 136	0.96
-2 km-C	ABA 143	0.97
-2 km-BL2		1.48
-2 km-BG1		0.04
-2 km-BG2		0.09
0 km-RE		2.04
4.2 km-L	ABA 177	0.86
4.2 km-F	ABA 168	2.09

We have identified four morphotypes of **ostracodes**:

- with smooth valves (including a significant number of juvenile forms),
- with longitudinal ridges: ? *Cistacythereis* sp. (Pl. 5, figs. 3-4),
- with reticulate ornaments: *Alocopocythere reticulata indoaustralica* HARTMANN, 1978 (Pl. 5, figs. 5-6),
- with a dorsal bulging and an accuminate posterior margin: *Gibboborchella* sp. (Pl. 5, figs. 1-2).

The last three species are characteristic of the "Muds with small pelecypod shells" facies.

Spirorbis is an annelid characterized by its small calcareous tube, always spired and fixed on one side (Pl. 2, figs. 1-2, 5-7; Pl. 3, fig. 1; Pl. 4, figs. 1 & 3). This fixing side moulds the shape of its holder perfectly and thus offers an exact image of the latter with its finer details (Pl. 2, fig. 5; Pl. 3, figs. 1-7; Pl. 4, figs. 2 & 4).

Chlorophyta are represented by one species: *Acetabularia caliculus* LAMOUROUX *in* QUOY & GAIMARD, 1824, which is still present in the area (GRANIER, 2012: Fig. 3.A-D). These algal remains are commonly found in the sediments in the form of hollow aragonitic tubes corresponding to the outer calcification of the algal thallus (GRANIER, 1995: Pl. 4, fig. 5-9; 2012: Fig. 5.A & 5.D; herein Pl. 1, figs. 4.a-c & 7), and less commonly in the form of fertile caps (GRANIER, 1995: Pl. 4, figs. 1-2, 4 & 10; herein Pl. 1, figs. 1-3) without fertile ampulae (GRANIER, 1995: Pl. 4, fig. 3). STROMENGHER *et al.* (2010: Fig. 17.g & 17.i) misinterpreted these tubes as "worm tubes (serpulids)". Fertile ampula are found as nuclei in some ooids (Fig. 7). From a paleoenvironmental perspective, ***Acetabularia*** grows on any rigid substrate, *i.e.*, on bedrocks or gravel beds, on shells (GRANIER, 2012: Fig. 3.A-D), and even on larger seaweeds, seagrasses or mangrove roots. It tolerates high salinity levels and, given its limited photosynthetic surface, it usually grows in water depths not exceeding five meters (DAWSON, 1966).

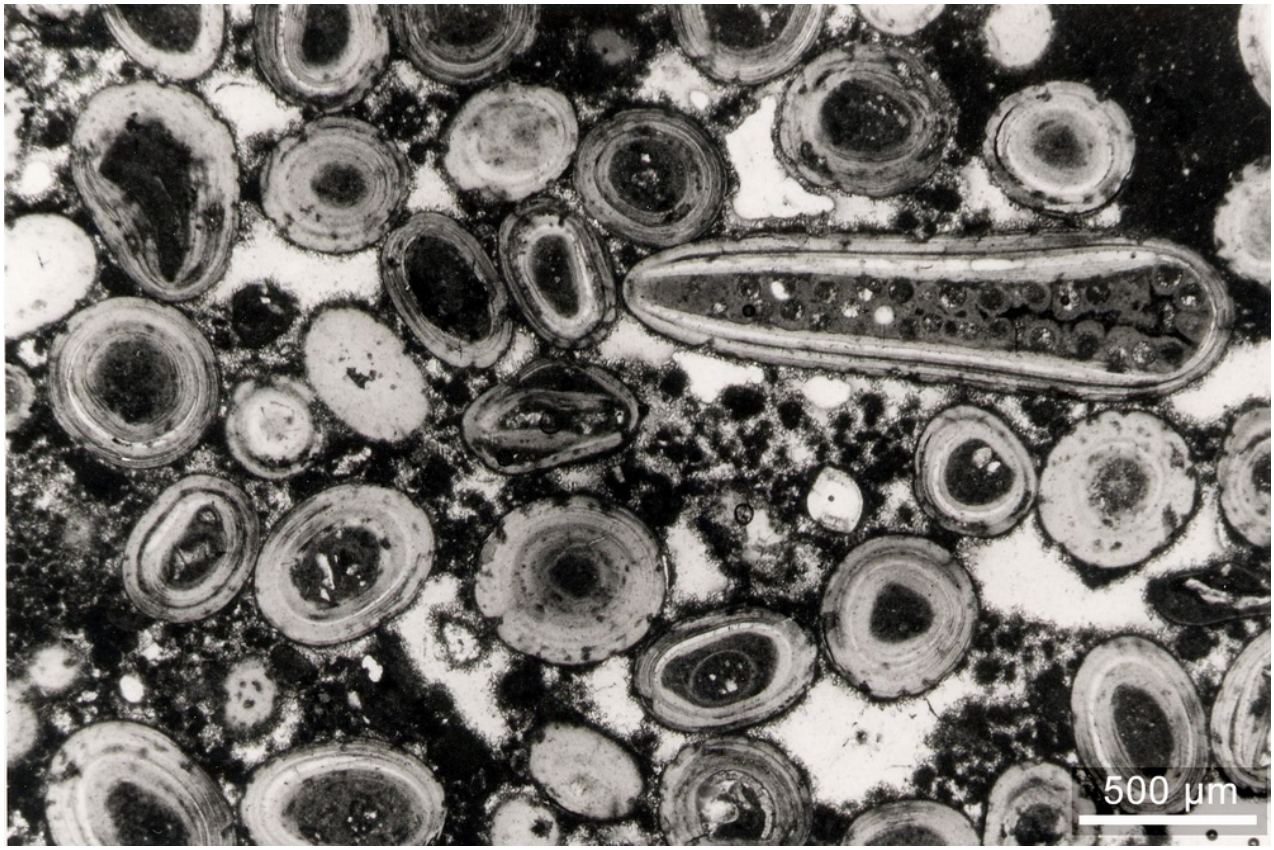

Figure 7: Fertile ampula of a Polyphysaceae (probably an *Acetabularia* sp.) as a nucleus of a Pleistocene ooid. Sample from a geotechnical core in Pleistocene material from the Abu Dhabi offshore.

A summary of the paleoecological preferences of the most representative benthic foraminifera (species or groups with similar paleoecological affinities) was compiled for the section studied. The information gathered includes, where available: paleobathymetry, microhabitat, oxygen preferences, temperature, and additional ecological data (Table 1). The paleoecological preferences of planktonic foraminifera with respect to surface water temperature and productivity were also summarized (Table 2).

4. The facies

Eight main facies types (5) and subtypes (3) were identified during field work:

- microbial mat, which grades laterally into microbial-laminated sediments,
- gypsum and enterolithic anhydrite (or ? bassanite),
- muds with small pelecypods,
- seagrass meadow facies,
- Potamid sands,
- Potamid beach-rock,
- washover fan coquina,
- aeolian sands.

4.1. The microbial mats

Occurrence of widespread microbial mats lining the intertidal flats of the Abu Dhabi emirate has been extensively described in the literature (*e.g.*, KENDALL & SKIPWITH, 1969a, 1969b; EVANS *et al.*, 1973; ALSHARHAN & KENDALL, 2003).

The defining feature of this facies is the occurrence of microbial (*i.e.*, cyanobacterial) laminae. The microbial-laminated appearance is more or less obvious depending on the ratio of organic laminae versus sedimentary laminae, on the amount of bioturbation, and the diagenetic processes among which *in situ* gypsum precipitation.

Granulometry: Grains of this facies are primarily arranged into two size categories (see Poster 10): those where grain sizes larger than 0.250 mm represent 20 to 30 % of the dry weight of the sediment (Samples ABA 129, 131, 133, and 165), and those where grain sizes larger than 0.063 mm (and smaller than 0.250 mm) represent 15 to 30 % of the dry weight of the sediment (Samples ABA 135, 137, 144, and 168).

Mineral composition: The microbial and the microbial-laminated sediments often contain 25 to 40 % aragonite with 5 % dolomite and 5 to 15 % calcite. However, exceptionally, some samples have mostly dolomite. This enrichment in dolomite apparently occurs to the detriment of the aragonite:

- 33 % of dolomite versus 0 % of aragonite in Sample ABA 129 (total 33%),
- 15 % of dolomite versus 10 % of aragonite in Sample ABA 160 (total 25%),
- 14 % of dolomite versus 16 % of aragonite in Sample ABA 137 (total 30%).

Halite presence may reach up to 30 %. Its highest percentages are always observed in these facies. Finally, both magnesian calcite and quartz are common although they never exceed 5 %.

Total Organic Carbon: The organic carbon levels of eight samples from this facies may be arranged into three groups:

- 0.3-0.6 % (*e.g.*, Sample ABA 137),
- 0.9-1.2 % (*e.g.*, Sample ABA 160),
- 1.8-2.1 % (*e.g.*, Sample ABA 129).

Allochems ranging in size from 0.250 to 2 mm: Intraclasts commonly represent 80 to 100 % of these grain sizes whereas extraclasts and bioclasts can reach 10 % and 20 %, respectively.

The bioclasts consist of remains of pelecypods and gastropods, bryozoans, worms (*Spirorbis*), ostracodes (those with smooth valves), foraminifers (*Peneroplis* and *Ammonia*), and green algae (*Acetabularia*). Exceptionally, one sample (ABA 135 with a TOC of 1.0 %) consists of 38 % bioclasts, half of them being *Peneroplis*. This makes it a close match with one sample (ABA 142) from the sediment immediately underlying the microbial mat, and suggests a mixture of both facies.

Remarks: Comparison of several diagrams of microbial mats shows that, as already pointed out by MONTY (1973), their mineralisation results more from biochemical precipitation than from the incorporation of detrital grains (*e.g.*, bioclasts). As a matter of fact, 80 to 100 % of the allochems are intraclasts, resulting from an *in situ* lithification. In thin section, these intraclasts consists of clotted micrite. In scanning electron microscopy (SEM), one sample (ABA 165) revealed many coccoid structures, 3 µm large in average, of cyanobacterial origin (Pls. 12-13).

4.2. Gypsum and enterolithic anhydrite (or ? bassanite)

Similarly to the previous facies, the widespread sabkhas of the Abu Dhabi emirate have been extensively described by several authors (*e.g.*, KENDALL & SKIPWITH, 1969a, 1969b; BUTLER *et al.*, 1982; ALSHARHAN & KENDALL, 2003).

This facies is characterized by the abundance either of gypsum crystals of various sizes and shapes or of anhydrite in the form of enterolithic layers.

Granulometry: As expected, particles finer than 63 µm in size, which includes the sulfate salts, are the most prevalent in this facies (Samples ABA 124, 125, 136, 141, 143, 147, 148, 149, 162 and 163) (see Poster 10).

Mineral composition: Gypsum and anhydrite represent 45 to 70 % of the sediment. For the most part, aragonite seems to be missing, but two samples out of eleven contain slightly more than 10% (Samples ABA 136 and 163). The same generally applies to dolomite, but four samples (Samples ABA 124, 136, 140 and 149) still contain a small amount. Quartz is either missing or present at trace levels. Only calcite occurs in all the samples analysed. High-magnesian calcite is missing, but low-magnesian calcite content ranges from 5 to 15 %.

Allochems ranging in size from 0.250 to 2 mm: They are either extraclasts or intraclasts. Extraclasts are found in the uppermost part of the gypsum and anhydrite layer (Samples ABA 124, 148, 149, and 163) and are thus probably of aeolian origin. Intraclasts of this facies are found in the lowermost part of the gypsum and anhydrite layer, next to the microbial-laminated layers (Samples ABA 130, 136, 142, 143, and 147) and therefore merely represent a diagenetic change of the microbial mat itself (Pl. 16).

The gypsum facies is clearly a diagenetic facies (as opposed to a depositional facies). In most cases, it developed to the detriment of the microbial mat (see MONTY, 1973, *inter alia*). Anhydrite occurred late as a replacement of gypsum as suggested by the occurrence of ghosts (*i.e.*, pseudomorphs) of gypsum crystals and all the transitional forms to a full replacement of gypsum, as already pointed out by ILLING *et al.* (1965).

Remark: Gypsum may fill former intergranular pores, including locally *Avicennia* mangrove roots, be present in calcareous sandy and pebbly sediments (*e.g.*, samples ABA 98 or 175), and form large crystals behaving like a poecilitic cement (Pl. 16, fig. 2).

4.3. Muds with small pelecypods

In the field, burrows are frequently reported from this predominantly muddy facies.

Granulometry: Besides the abundance of small pelecypods and foraminifers (*Peneroplis* and *Ammonia*), and the activity of burrowing organisms, which are the main producers of faecal pellets, the sediment is either a sandy to silty mud (Samples ABA 94, 132, 139, 142 and 146) or a muddy sand (Samples ABA 123, 161, 169, 173bis and 176), eventually pebbly (see Poster 10).

Mineral composition: It is variable, apparently depending on the vertical position of the sample within the facies:

- shallower (Samples ABA 95, 100, 123, 132, 139 and 146), aragonite varies from 20 to 40 % and halite from 10 to 20 %;
- deeper (Samples ABA 161, 169, 173, 173bis, 176 and 177), aragonite varies from 40 to 60 % and halite is lower than 5 %. Such fluctuations may result either from the original mineral composition or from diagenetic changes.

Magnesian calcite rarely exceeds 5 % (Sample ABA 177); calcite varies from 5 to 15 %. Dolomite may be missing (Samples ABA 142, 169 and 173), or may reach significant levels (*i.e.*, up to 22 % for samples ABA 132 and 146). Quartz is

always very scarce (less than 5 %). Exceptionally, one sample (ABA 142) contains 59 % gypsum.

Total Organic Carbon: The five samples analysed (ABA 142, 146, 161, 176 and 177) have values ranging between 0.2 and 0.8 %.

Allochems ranging in size from 0.250 to 2 mm: Within this range of grain sizes there are lumps, bioclasts and faecal pellets, which may be common (up to 5 %) or even abundant (15-20 %). The bioclasts consist mostly of pelecypods, on the one hand, and of foraminifers, on the other hand. The latter are *Peneroplis planatus* and *Ammonia beccarii*. Rather uncommon forms are exclusively or almost exclusively found in this facies. This is particularly true for *Miliammina fusca* (BRADY, 1870), a Miliolidae with an agglutinated test, and some ostracodes: *Alocopocythere reticulata indoaustralica* HARTMANN, 1978 (Pl. 5, figs. 5-6), ? *Cistacythereis* sp. (Pl. 5, figs. 3-4) and *Gibboborchella* sp. juv. (Pl. 5, figs. 1-2).

Remark: This facies is close to the "lamellibranch mud - type no. 10" of WAGNER and van der TOGT (1973).

There are actually two foraminiferal subfacies: one with numerous *Peneroplis* and few *Ammonia* (samples ABA 142, 161, 169, 173, 173bis and 177) and the other inversely proportional (samples ABA 123, 132, 139 and 146) that respectively correspond to the deeper and shallower samples in the various sections studied. Thus it is highly likely that changes in the mineral composition reported above for this type of facies are largely determined by their original skeletal composition.

4.4. Seagrass meadow muds

Seagrass meadows of the Abu Dhabi lagoons are documented in the literature (*e.g.*, EVANS *et al.*, 1973).

In the field sections, this facies is primarily distinguished from the surrounding more or less sandy and pebbly muds by the crowding of root traces and by the occurrence of *Anodontia* (Lucinid bivalve mollusc) shells fossilized in their living position.

Only two samples (ABA 140 -1.6 km- and ABA 177 -4.2 km-) were collected in this facies. All their key features, *i.e.*, mineral composition (including the clay minerals), TOC, granulometry, and nature of the sand-sized allochems, significantly differ.

Remark: An additional sampling in living seagrass meadows (ABA 383, 384 and 406) suggest that there is no unique facies for seagrass meadows. These seagrasses can grow on any soft substratum, either muddy or sandy and even slightly pebbly, and do not significantly modify it. They merely introduce a subfacies that may be difficult to distinguish from the surrounding facies as there is no specific mineral, biological or organic signature (other than root tracks) for this type of environment.

4.5. Potamid sands

Occurrences of Potamid sands in the Abu Dhabi lagoons are common in the literature (*e.g.*, EVANS *et al.*, 1973).

These calcareous sands are characterized by the abundance of *Cerithideopsilla conica* (BLAINVILLE, 1829), a Potamid gastropod that has a wide range of salinity tolerance from freshwater to hypersaline environments (PLAZIAT, 1993).

Granulometry: 70 to 80 % of the sediment consists of silt and sand (Samples ABA 102, 150 and 173) (see Poster 10).

Mineral composition: Aragonite represents 50 to 60 % of the sediments and calcite only 5 to 15 %. Dolomite is missing. Magnesian calcite, halite and quartz represent 5 % each, on average.

Clay minerals: One sample (ABA 173) was analysed. Clay minerals include 38 % attapulgite, 31 % illite, 16 % kaolinite, and 15 % chlorite.

Allochems ranging in size from 0.250 to 2 mm: They consist of bioclasts, lumps and intraclasts. The bioclasts comprise remains of gastropods and pelecypods, ostracodes (those with smooth valves), foraminifers (*Peneroplis* and *Ammonia*), and green algae (*Acetabularia*). The common occurrence of epiphytic faunas, such as some worm (*Spirorbis*) and bryozoan calcitic tests, is evidence for large seaweeds or seagrasses that were not fossilized.

Remark: This facies is close to the "gastropod sand - type no. 6" of WAGNER and van der TOGT (1973). The components of the intraclasts and lumps are bound together by a fibrous fringing cement consisting mostly of aragonite needles (Pl. 15, figs. 5-6).

4.6. Potamid beach-rocks

Such beach-rocks are reported from areas next to Abu Dhabi island (*e.g.*, EVANS *et al.*, 1973) and from Khor al Bazam (*e.g.*, ALSHARHAN & KENDALL, 2003).

These layers record early lithification. We identified at least three of them: two in a lower position and one in an upper position. However, only the upper one was sampled (ABA 145, 167, 172, 174 and 175).

Mineral composition: Aragonite represents 45 to 65 % of the sediments and calcite only 5 to 10 %. Dolomite occurs in three out of four samples and reaches a maximum of 10 %. Magnesian calcite, halite and quartz represent 5 % each, on average.

Allochems ranging in size from 0.250 to 2 mm: These allochems are similar to the assemblage found in the Potamid sands, *i.e.*, they consist of bioclasts, lumps and intraclasts. The components of the lumps are commonly peloids, *i.e.*, ovoid micritic allochems without any internal structure. Most often such grains result from the micritization of bioclasts. Exceptionally, we also found micritic ooids in this facies. These

ooids and the peloids are both aragonitic. The primary distinction between them is that cortices, *i.e.*, concentric structures, are visible in the ooids (Pl. 11, figs. 4-5) but are missing in the peloids.

Texture: The Potamid beach-rock is either a grainstone of peloidal lumps and foraminifers (less than 10 % grains larger than 2 mm) or a gastropod floatstone with grainstone matrix.

Remark: Lithification results from cementation by radially-arranged fibers of aragonite (Pl. 14, fig. 7). The mineral compositions of both the Potamid sands and the Potamid beach-rocks are almost similar. The only difference lies in the occurrence of dolomite in the lithified layers of the Potamid beach-rocks. The coarse components are the same. Thus, both facies correspond to the same depositional environment. For instance, one sample (ABA 171), the gravel-sized allochems of which represent more than 60% of the total dry weight, corresponds to an early stage of lithification of these Potamid sands. The lesser or greater extent of lithification is the sole responsible for the identification of a diagenetic subfacies: the beach-rocks.

4.7. Washover fan coquina

These coarse bioclastic sands are characterized by the occurrence of a cross-bedding with low-angle laminae (5 to 10°) inclined toward the lagoon. Two coquina ridges are found in the eastern end of the Mussafah channel transect, in the first 200 meters of the transect.

Granulometry: Allochems larger than 0.250 mm (medium and coarse sands, and gravels) represent more than 60% of the total dry weight (samples ABA 98, 121, 127 and 128).

Mineral composition: Aragonite represents 55 to 70 % of the sediments and calcite never exceeds 10 %. Dolomite is missing. Magnesian calcite was identified in one sample only (ABA 121). Halite and quartz are present but they never exceed 5 % each. Exceptionally, in this facies, one sample (ABA 98) contains 22 % gypsum.

Allochems ranging in size from 0.250 to 2 mm: Bioclasts represent more than 60 % of this grain-size category. The remaining allochems are intraclasts made of more or less cemented bioclasts. On average there are 30 % of both gastropod and pelecypod shells, from 10 to 15 % foraminifers (three quarters of them are *Peneroplis*), 10 % *Acetabularia*, from 5 to 10 % *Spirorbis*, and up to 5 % bryozoans.

Remark: According to REINECK & SINGH (1973), "the washover fan is made up of several superimposed sandy blankets of successive whashover fans (...). Each sandy blanket begins with a shell-rich layer, which possesses an erosive contact to the lower sediments. In the shelly horizon shells of macro-invertebrates from different biocenoses are mixed together. Then a sandy layer follows with well developed evenly laminated sand". That definition matches the description of the material studied, *i.e.*, a poorly sorted assemblage of shells including *Brachidontes*, *Tellina*, *Cerithium*, *Mitrella*, Potamids, Trochidae, *etc.*

4.8. Aeolian sands

In the field they consist partly of a modern (uppermost Holocene) sand blanket (sample ABA 164) and partly of the Pleistocene sandy substratum.

Granulometry: Fine sand, *i.e.*, with grain sizes ranging from 0.125 to 0.250 µm, represents from 40 to 55 % of the total dry weight for samples from the unconsolidated Pleistocene cross-bedded sands (samples ABA 96, 104, 166 and 170). Silts prevail in both the massive Pleistocene sands (sample ABA 97) and the modern aeolian blanket (sample ABA 164).

Mineral composition: This facies is characterized by the occurrence of 40 to 50 % calcite and 10 to 15 % quartz, plus 5 % feldspars, bringing the amount of siliciclastics to 15-20 %. Magnesian calcite is missing. Dolomite may reach or surpass 5 %. Halite represents 5 % in average. One sample - one of the Holocene sand (ABA 164) - contains 7 % anhydrite.

Clay minerals: Only two samples (ABA 97 and 170) were analysed for clay.

The clay mineral composition of the first sample (ABA 97), which corresponds to the finer Pleistocene sediment (silt), consists of 40 % attapulgite, 41 % montmorillonite, 14 % kaolinite, and 5 % chlorite.

The second sample (ABA 170), from the coarser Pleistocene sediment (fine sand), contains exclusively kaolinite (99 %).

As a distinguishing criterion, in relation to the other samples analysed, both samples share the absence of illite. In addition they contain very little, if any, chlorite.

Allochems ranging in size from 0.250 to 2 mm: They almost exclusively consist of "rounded grains". In petrographic thin sections, they appear to be calcitic ooids, bioclasts and extraclasts. These bioclasts are echinoid spines, various remains of gastropods and pteropods, calcareous red algae (Corallinales and Sporolithales), and foraminifers (primarily Textulariidae, Lituolidae and Lenticulinidae, and secondarily *Peneroplis* and forms close to Acervulinidae).

5. Some notes on "algae"

As reported above, "algae" occur in most facies. However there are some forms that we have not mentioned yet:

Coccolithophorids: Under Scanning Electron Microscopy, specimens of *Miliammina*, *i.e.*, a genus ascribed to the Miliolidae but with an agglutinated test, revealed that few coccoliths, *i.e.*, the disc-shaped plates the assembly of which

forms a coccosphere around the planktonic unicellular Haptophyta alga, are parts of the foraminiferal shell.

Diatoms: Frustules, *i.e.*, the siliceous valves around Bacillariophyta unicellular algae, either recrystallized as calcite or in the form of empty molds, were observed on the fixation face of tubes of *Spirorbis* (Pl. 3, figs. 2-5 &7; Pl. 4, fig. 2). In our material, we identified pennate forms, which have benthic life habits and commonly grow on larger algae.

Rhodophyta: Very few sections ascribed to Rhodophyta are observed in the Holocene lithified samples. Hoewever, besides the diatom frustules (Pl. 3, figs. 2-5 & 7; Pl. 4, fig. 2), we identified *Lytophyllum*-like structures on the fixation face of a *Spirorbis* tube (Pl. 4, figs. 1-4). David M. JOHN (personal communication, May 6, 2017) suspects one of them "might well be" *Lithophyllum kotschyanum* UNGER, 1858, which "is certainly also reported to be far the most common species elsewhere along the southern coast of the Arabian Gulf" (see JOHN, 2012), but he also adds it is "impossible to be certain" from the image.

In addition, Rhodophyta remains, including geniculate coralline algae (Pl. 10, fig. 6), are commonly found inside "rounded grains", *i.e.*, inside the small Pleistocene (?) extraclasts.

Another algal specimen observed in one sample (ABA 129) looks like red algae, *i.e.*, a pluricellular structure with pit connections (Pl. 14, fig. 1). Brian WYSOR (personal communication, April 29, 2016) suggested it could be *Bostrychia arbuscula* HARVEY, 1855.

Cyanobacteria: They are the main contributors to the microbial mats (MONTY, 1973, *inter alia*). David M. JOHN (personal communication, May 13, 2016) suggested that some of our specimens (Pl. 14, figs. 2-3) resemble interwoven filaments of *Coleofasciculus chthonoplastes* (GOMONT, 1892). As is documented in our material by the intraclasts (Pls. 12-13), lithification results more from biochemical precipitation processes than from grain trapping. In association with fungi, some cyanobacteria also play a destructive role (*e.g.*, RIOULT & DANGEARD, 1976), *i.e.*, bioerosion (Pl. 11, fig. 3; Pl. 14, fig. 6).

Large (brown, red or green) **seaweeds**: With their anchoring organs or rhizoids, they colonize either pebbly or rocky substrates. Although they are not fossilized, these forms played a considerable role in sedimentation:

- they form in turn the substrate of many epiphytic organisms (*Acetabularia*, pennate diatoms, *Spirorbis*, *Peneroplis*, *etc.*),
- they provide a source for organic matter.

Seagrasses: They are not algae, but phanerogams with roots. They commonly colonize loose, muddy or sandy, substrates. In the same way as for the large seaweeds, they form in turn the substrate of many epiphytic organisms (BEAVINGTON-PENNEY *et al.*, 2004).

6. Discussion and conclusions

Among the eight facies described above, two are of diagenetic origin:

- Gypsum and enterolithic anhydrite (§ 4.2.):

This diagenetic facies affects the uppermost half meter of sediments in the eastern part of the transect and gets gradually thinner towards the lagoon. It is partly controlled by the modern topography (Poster 1). This type of diagenesis affects both the Holocene aeolian sands (§ 4.8.) and the microbial mats (§ 4.1.). From the lagoon up the coastal sebkha, gypsum is gradually replaced by anhydrite. In addition, it appears that dolomite always occurs as a replacement of aragonite, an unstable polymorph of calcium carbonate $CaCO_3$: see, for instance, the mineral composition of the microbial mats and also SEM photomicrographs of faecal pellets (*e.g.*, Pl. 8, fig. 6);

- Potamid beach-rocks (§ 4.6.):

They results from the early lithification of Potamid sands (§ 4.5.) by aragonitic cement in a marine phreatic setting. There are several beach-rocks clearly distinguishable on the basis of their position and tilt (Poster 1). The lower beach-rocks are partly sub-horizontal whereas the upper beach-rock is sloping downwards toward the lagoon.

Furthermore the seagrass meadow muds, which are characterized by root tracks, are merely a subfacies of the muds with small pelecypods. As already discussed above, both facies only differ by their outer appearances: allochems, granulometries and mineral compositions are similar. The reconstruction of the Mussafah channel transect allows us to identify two discrete seagrass meadows (Poster 1):

- a lower meadow, the location of which may be related to the close occurrence of a small Pleistocene slope,
- an upper meadow, the location of which may be related to the close occurrence of wash-over crests.

The **virtual vertical sequence of facies** comprises from base to top:

- seagrass meadow muds,
- muds with small pelecypods,
- Potamid sands,
- microbial mats,
- aeolian sands, roughly corresponding to laterally adjacent facies belts from the shallow lagoon to the tidal flat. It would be a perfect illustration of the WALTHER's law if there was no sedimentary break!

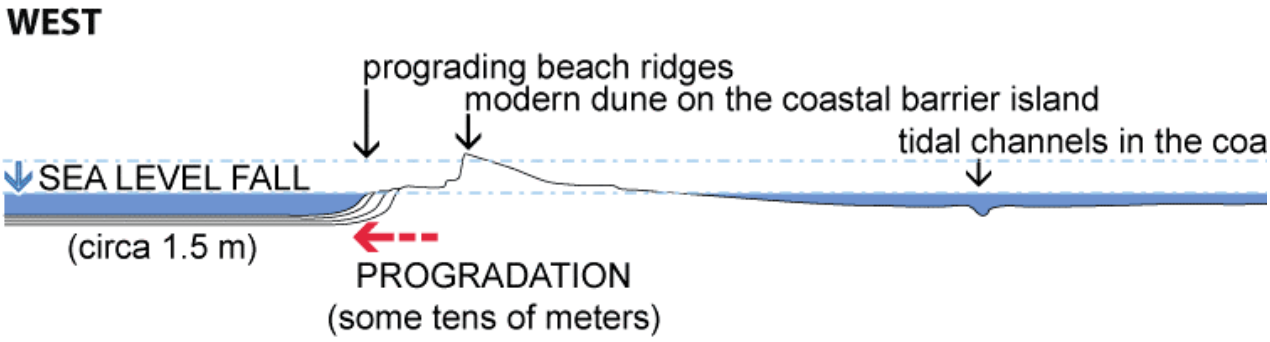

Figure 8: The model (see text for comments).

Although differential compaction of muds and calcareous sands due to mud dewatering and sand cementation caused difficulties in the sequential interpretation, three discrete sedimentary patterns have been identified in the sequence of facies observed on the Mussafah channel transect (Poster 1):

1) a **transgressive, retrogradational, deepening upward pattern**: It starts at a sharp contact of a relict microbial mat on the underlying Pleistocene aeolian sands. This basal organic-rich layer is followed by Potamid sands, then by muds with small pelecypods. The full sequence can be observed at sections located from 0 km to 1 km from the transect origin. Beyond these sections the basal microbial mat is missing. From 2.2 km to 4.4 km, lower seagrass meadow muds are interposed between Potamid sands and muds with small pelecypods. Both thick Potamid sands and seagrass meadow sediments pinch out landward due to a topographic change between 2.0 km and 2.4 km from the transect origin. Note that the transgression here was probably not smooth and gradual but rather a pulsed phenomenon. The maximum of the transgression is possibly recorded by the washover fan coquina on the eastern (landward) side of the transect (Poster 1);

2) a **regressive, progradational, shallowing upward pattern**. KENIG (2011) referred to a "regressive microbial mat" but did not enter into the details regarding the sequence of events. This regressive trend is clearly divided into two parts:

2A) a **normal regression**. This part is not easy to characterize due to dominantly muddy facies. However, it ends locally, *i.e.*, from 0.6 km to 1.8 km from the transect origin, with the upper seagrass meadow muds;

2B) the direct superposition of microbial mats on these upper seagrass meadow muds without interposition of Potamid sands is indicative of a significant downward shift of facies, *i.e.*, it is the mark of a **forced regression**. At sections located from 3.2 km to 4.4 km from the transect origin, Potamid sands are overlain by microbial mats, which in turn are overlain by the Holocene aeolian sands. Beyond the 5.8 km mark, lagoonal muds are interposed between Potamid sands and microbial mats.

In conclusion, both microbial mats, the lower and the upper, have discrete significances in terms of relative sea-level trends. The lower microbial mat is the mark of a transgression (KENIG, 2011) whereas the upper microbial mat is the mark of a forced regression.

The **relative sea-level fall** corresponding to this last forced regression can be estimated on the basis of the position of the upper microbial mats. It is at least 1.6 m, which is the topographic difference of these microbial maps at the 0.4 km and 7.2 km marks.

The amplitude of a **transgression** and that of a **regression** are estimated on the basis of the horizontal shifts, respectively landward and seaward, of the **shoreline** (*i.e.*, the mean high water line). It can be approached through peculiar sedimentary facies found in shallow-water settings that provide evidence for water encroachment along the innermost side of the lagoon. Considering that microbial mats thrive in the upper intertidal zone, the shoreline shift during the regressive interval can be estimated soley on the basis of the location of the upper microbial mats. These upper microbial mats are found in almost all sections along the transect, starting from the - 2 km mark. Consequently, the last forced regression corresponds at least to a 5 km lateral shift, a result that is in general agreement with observations made by geologists who preceded us in the same area (SHEARMAN, 1966, *inter alia*).

In the case of the Abu Dhabi lagoons, which are sited on the southern margin of an epicontinental sea, the amplitude of the **progradation** and that of the **retrogradation** in this ramp system can be estimated on the basis of the horizontal shifts, respectively lagoonward and (open) seaward, of the **rollover line** of the coastal oolitic barrier (*i.e.*, the mean low water line on the open marine side of the barrier). The last forced regression led to a limited lateral seaward shift of the modern oolitic barrier in the range of some tens of meters only. The existence of the barrier and its effectiveness at protecting and isolating the lagoon have probably significantly

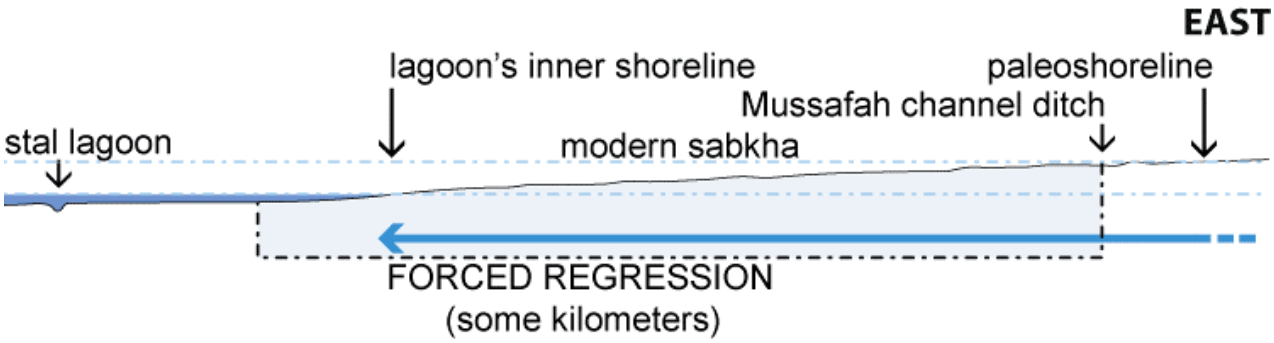

impacted the depositional environments and the nature of the sediments in the Mussafah area during the Holocene transgressive-regressive cycle. According to some authors (PURSER & EVANS, 1973: Fig. 11), the coastal barrier settled on a preexisting ridge, *i.e.*, a fossil relative high, which "has influenced all subsequent physiographic processes" (KASSLER, 1973). However, further investigations on the coastal barrier and under the lagoon waters are required to test further this hypothesis.

Despite the relative incompleteness of our study, *i.e.*, some subject areas have not been fully addressed and we were missing absolute radiocarbon datings, our sedimentological analyses have documented a transgressive-regressive sequence of facies in relation to relative sea-level changes. Recently, STROMENGHER *et al.* (2010) who investigated a 0.7 km long transect (compared our 9 km transect) provided these invaluable radiocarbon ages. According to these data, the Holocene sediments of the upper part of our transect range in age from 6,600 ± 40 to 4,950 ± 60 years BP (minimum range) and the youngest Pleistocene aeolian sandstones are dated at 23,490 ± 130 years BP. This information helps to better constrain our interpretation in time. The reversal point of the relative sea-level rise (transgression and normal regression) to the fall (forced regression) takes place somewhere between 5,000 and 6,500 BP. That is in agreement with several reports that places it at about 6,000 years BP (geological reports) or at about 4,000 years BC (archaeological reports) at the "climax of the Flandrian transgression" (BARTH, 2001, *inter alia*). The following relative sea-level fall is estimated to be not less than 1.5 m (1.8 m according to KENIG, 2011) with an associated seaward shift of the shoreline of some 5 km (forced regression), whereas the coeval seaward shift of the rollover line of the lagoon barrier might have been of some tens of meters only (effective progradation): Fig. 8.

Acknowledgements

This publication is dedicated to the memory of the late Philippe BOUSQUET. The authors would like to thank TOTAL for having granted permission to publish this paper. Researchers participating to the 1986 and 1987 field work were F. BALTZER, R. BOICHARD, M. HUC, F. KENIG, J.-L. OUDIN, J.-C. PLAZIAT and B. PURSER. Except for the X-ray mineralogical analyses undertaken by G. JOUSSON, all laboratory analyses were conducted by B. GRANIER. The authors are also very grateful to Phil SALVADOR who carefully polished the English text of this manuscript, J.-C. PLAZIAT who provided invaluable additional information on the coastal sedimentology of Abu Dhabi, Francesco SCIUTO who identified the ostracodes, and to David M. JOHN, Paulo Antunes HORTA, Curt M. PUESCHEL, Carlos G. VÉLEZ and Brian WYSOR who provided valuable information on some algae. SEM photos from Plate 4 were taken by Hermes BRITO at the UNESPetro, Rio Claro, SP, Brazil.

Figures 9-14 are part of a previously unpublished contribution of Jean-Claude PLAZIAT. They comprise a set of photos taken during the last field mission in February 1987.

Bibliographic references

ALSHARHAN A.S. & KENDALL C.G.St.C. (2003).- Holocene coastal carbonates and evaporites of the southern Arabian Gulf and their ancient analogues.- *Earth-Science Reviews*, vol. 61, no. 3-4, p. 191-243.

BALTZER F., KENIG F., BOICHARD R., PLAZIAT J.-C. & PURSER B.H. (1994).- Organic matter distribution, water circulation and dolomotization beneath the Abu Dhabi sabkha (United Arab Emirates).- *International Association of Sedimentology*, *Special Publication*, vol. 21, p. 409-427.

BARTH H.-J. (2001).- Understanding of coastal fluctuation at the Arabian Gulf leading to the "lost city of Gerrha"?- *Palaeoecology of Africa*, vol. 27, p. 291-303.

BARTH H.-J. & KHAN N.Y. (2002).- Biogeophysical setting of the Gulf. *In*: ABUZINADA A.H., BARTH H.-J., KRUPP F., BÖER B. & AL ABDESSALAAM T.Z. (eds.), Protecting the Gulf's marine ecosystems from pollution.- Birkhäuser Verlag, Bâle, p. 1-21.

BEAVINGTON-PENNEY S.J., WRIGHT V.P. & WOELKERLING W.J. (2004).- Recognising macrophyte-vegetated environments in the rock record: A new criterion using "hooked" forms of crustose coralline red algae.- *Sedimentary Geology*, vol. 166, p. 1-9.

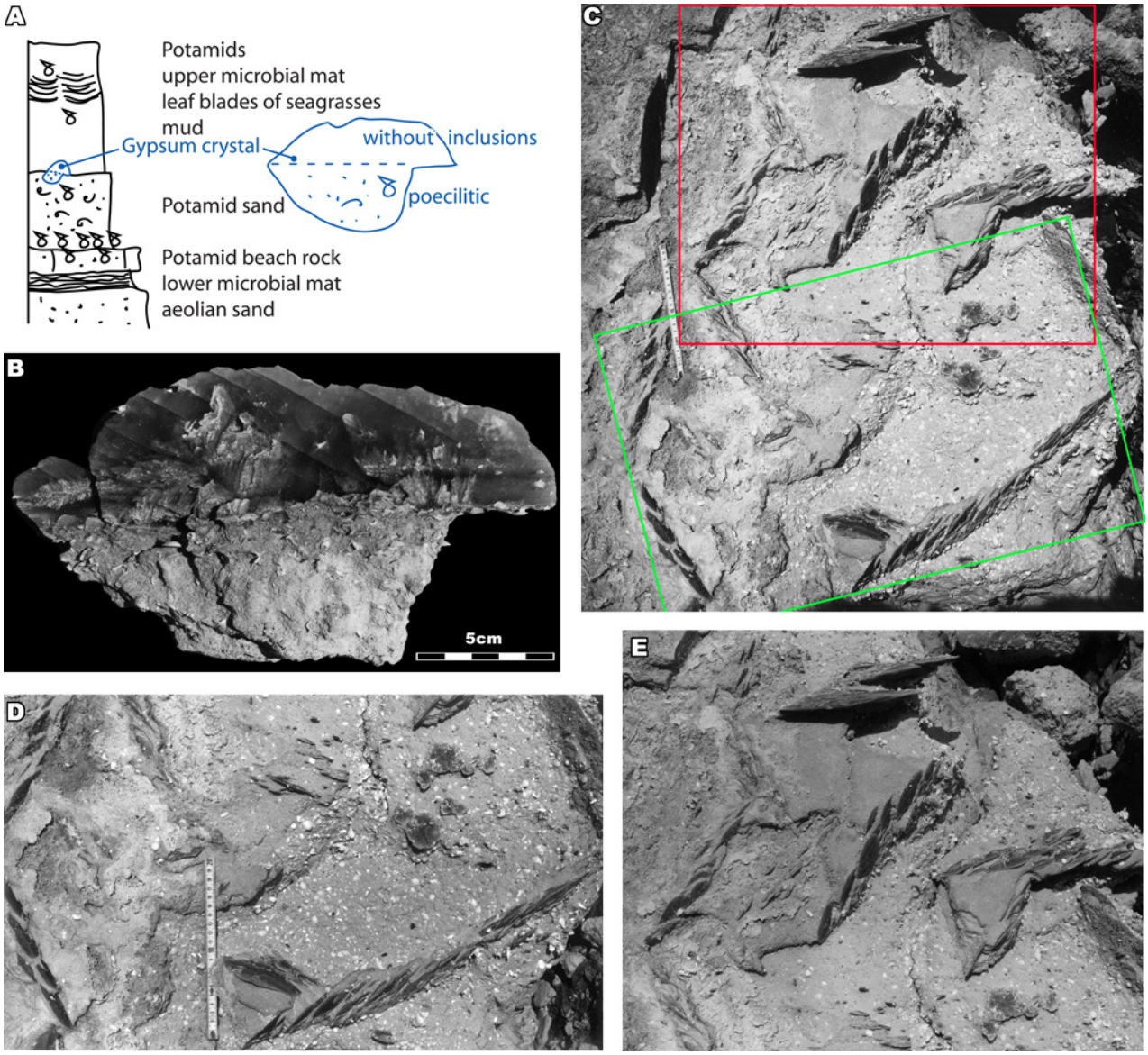

Figure 9: [by courtesy of Jean-Claude PLAZIAT, Mussafah, February 1987]**: A)** a section near the eastern end of the Mussafah channel displaying typical facies including Potamid sands and beachrock, as well as the lower and the upper microbial mats; **B)** detail of a syntaxial gypsum crystal, with inclusions (poecilitic) and without; **C-E)** large gypsum crystals at the boundary between the mud and the bioclastic sand. D corresponds to the green frame of C, and E to the red frame.

BERGER S. (2006).- Photo-atlas of living Dasycladales.- Carnets de Géologie, Madrid, Book 2006/02 (CG2006_B02), ISBN 2-916733-01-9, 348 p.

BUTLER G.P. (1969).- Modern evaporite deposition and geochemistry of coexisting brines, the sabkha, Trucial Coast, Arabian Gulf.- *Journal of Sedimentary Petrology*, vol. 39, no. 1, p. 70-89.

BUTLER G.P., HARRIS P.M. & KENDALL C.G.St.C. (1982).- Recent evaporites from the Abu Dhabi coastal flats. *In*: Deposional and diagenetic spectra of evaporites.- Core workshop, Calgary, 26-27 juin 1982.- *Society of Economic Paleontologists and Mineralogists*, *Special Publications*, Tulsa, vol. 3, p. 33-64.

DAWSON E.Y. (1966).- Marine Botany.- Holt, Rinehart and Winston, New-York, 326 p.

EVANS G., KINSMAN D.J.J. & SHEARMAN D.J. (1964).- A reconnaissance survey of the environment of recent carbonate sedimentation along the Trucial Coast, Persian Gulf. *In*: STRAATEN L.M.J.U. van (ed.), Deltaic and shallow marine deposits.- 6th International Sedimentological Congress, 1963.- *Developments in Sedimentology*, Elsevier, Amsterdam, 1, p. 129-135.

EVANS G. & KIRKHAM A. (2002).- Part I Distribution of sabkhat within the Arabian peninsula and the adjacent countries. *In*: BARTH H.-J. & BÖER B. (eds.), Sabkha ecosystems.- Kluwer Academic Publishers, Dordrecht, p. 7-20.

EVANS G., KIRKHAM A. & CARTER R.A. (2002).- Quaternary development of the United Arab Emirates coast: New evidence from Marawah Island, Abu Dhabi.- *GeoArabia*, Manama, vol. 7, no. 3, p. 441-458.

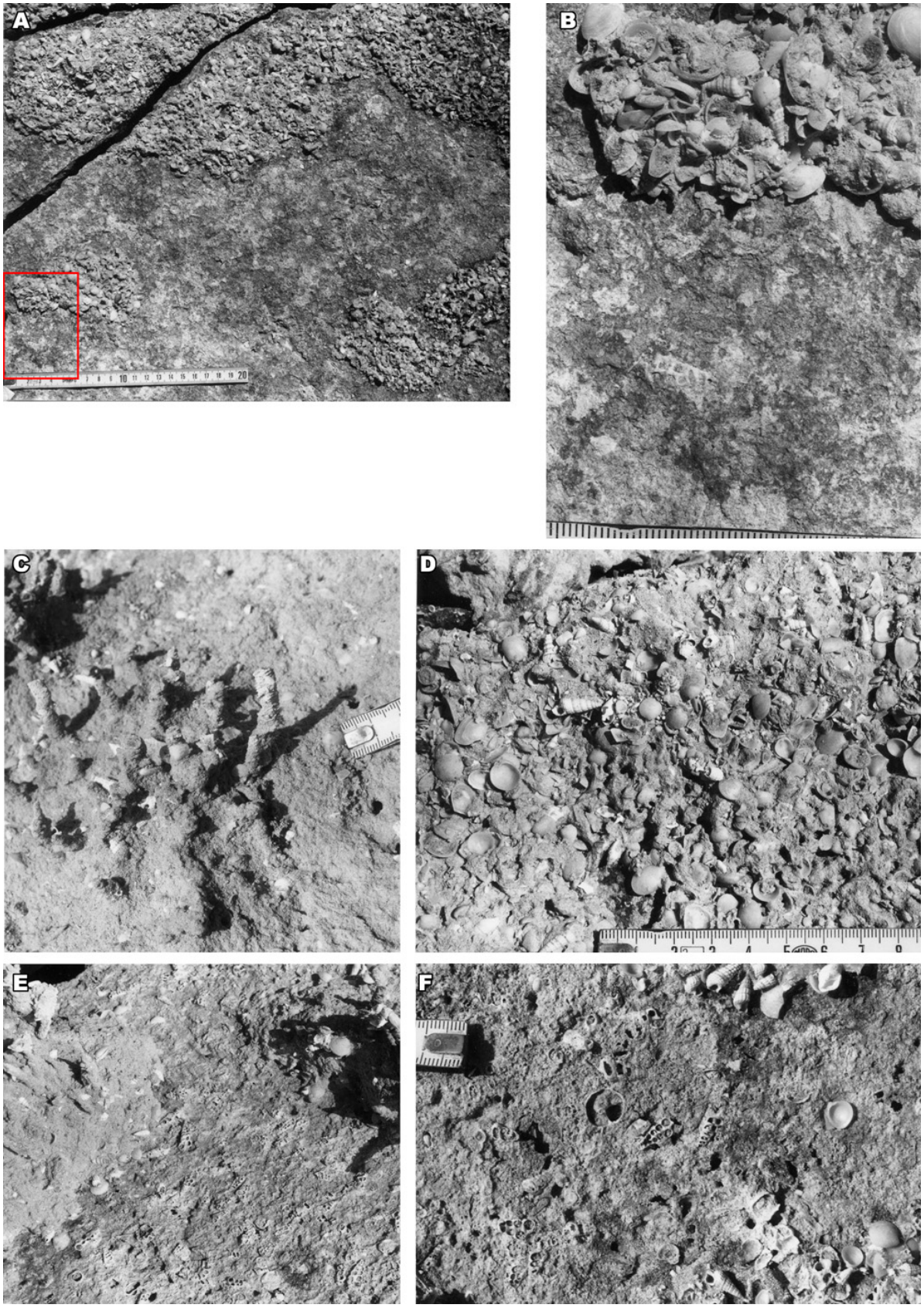

Figure 10: [by courtesy of Jean-Claude PLAZIAT, Mussafah, February 1987]**: A-F)** top of the Potamid beach-rock. B corresponds to the red frame of A. Erosion of the Potamid shells (A-B, F) documents an early lithification followed by mechanical abrasion. By contrast cementation of the more diverse assemblage of shells found above the erosional surface (A-B, D) is probably not an" early diagenetic event", *i.e.*, lithification took place within the sedimentary pile; **C)** gypsiferous open burrows in the Potamid sand above the Potamid beach rock; **E)** gypsiferous open burrows (as in C) and surficial erosion of the early lithified Potamid beach rock.

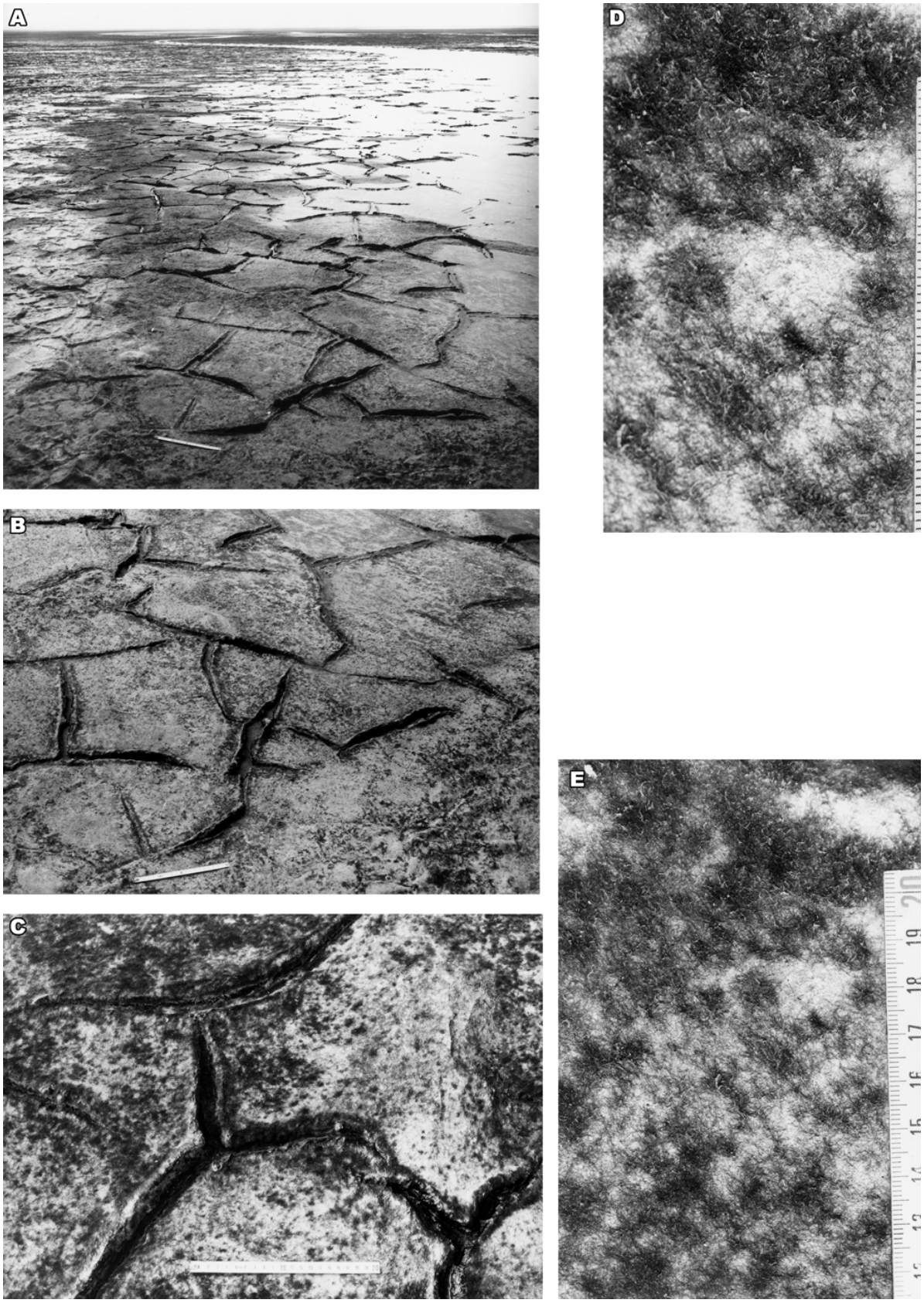

Figure 11: [by courtesy of Jean-Claude PLAZIAT, Mussafah, February 1987]**: A)** microbial mats infilling on bottom of a residual pond in a former tidal channel; **B)** healed desiccation cracks in the living microbial mat; **C-D)** smooth to felted surficial appearance of the microbial mat.

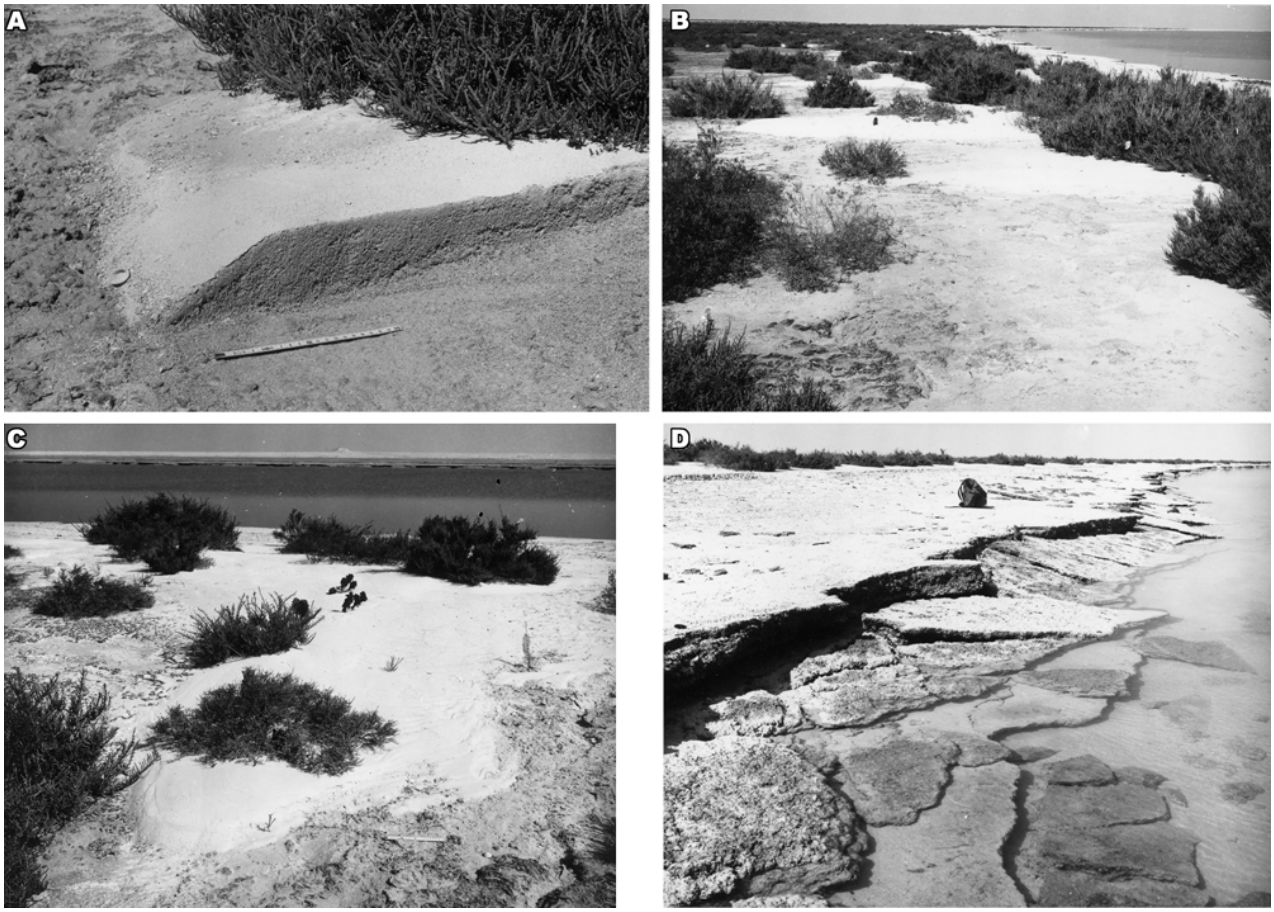

Figure 12: [by courtesy of Jean-Claude PLAZIAT, Mussafah, February 1987]**: A)** The upper Potamid beach-rock at the edge of Mussafah channel near 7.2 km mark; **B-C)** modern sand blankets created by sediment transport from the channel to its edges (washover fans) during storm events. There, plants bearing yellow flowers (*cf.* orobanche / broom-rape) are parasites of *Salicornia* (*Arthrocnemum* spp.), a well-known halophyte plant.

EVANS G., MURRAY J.W., BIGGS H.E.J., BATE R. & BUSH P.R. (1973).- The oceanography, ecology, sedimentology and geomorphology of parts of the Trucial Coast barrier island complex, Persian Gulf. *In*: PURSER B.H. (ed.), The Persian Gulf.- Springer Verlag, Berlin, p. 233-277.

FOLK R.L., CHAFETZ H.S. & TIEZZI P.A. (1985).- Bizarre forms of depositional and diagenetic calcite in hot-spring travertines, central Italy. *In*: SCHNEIDERMANN N. & HARRIS P.M. (eds.), Carbonate cements.- *Society of Economic Paleontologists and Mineralogists*, *Special Publications*, Tulsa, vol. 36, p. 349-369.

HOTTINGER L., HAMICZ E. & REISS Z. (1993).- Recent Foraminiferida from the Gulf of Aqaba, Red Sea.- *Slovenska akademija znanosti in umetnosti*, Ljubljana, Razred za naravoslovne vede, (Classis IV: *Historia naturalis*), Dela * Opera, 33, 179 p. (230 Pls.).

HUGHES CLARKE M.W. & KEIJ A.J. (1973).- Organisms as producers of carbonate sediment and indicators of environment in southern Persian Gulf. *In*: PURSER B.H. (ed.), The Persian Gulf.- Springer Verlag, Berlin, p. 33-56.

GRANIER B. (1988, unpublished).- Étude pétro-sédimentologique de la coupe du Canal de Mussafah (Abu Dhabi - Émirats Arabes Unis).- TOTAL-Compagnie Française des Pétroles, Rapport Laboratoires, Pessac, no. RL 4324, 18 p.

GRANIER B. (1995).- The genus *Actinoporella* (GÜMBEL in ALTH, 1881) and its representatives. A review. *In*: Proceedings of the International Symposium and Field-Meeting "Alpine Algae '93".- *Beiträge zur Paläontologie*, Vienna, no. 19 (1994), p. 113-127.

GRANIER B. (2012).- The contribution of calcareous green algae to the production of limestones: A review. *In*: BASSO D. & GRANIER B. (eds.), Calcareous algae and the global change: from identification to quantification.- *Geodiversitas*, Paris, vol. 34, no. 1, p. 35-60.

GRANIER B. & DIAS-BRITO D. (2015).- End of a modern geological myth: there are no rudists in Brazil! Paleobiogeographic implications.- *Carnets Geol.*, Madrid, vol. 15, no. 11, p. 123-136.

ILLING L.V., WELLS A.J. & TAYLOR J.C.M. (1965).- Penecontemporary dolomite in the Persian Gulf.- *Society of Economic Paleontologists and Mineralogists*, *Special Publications*, Tulsa, vol. 13, p. 89-11.

JOHN D.M. (2012).- Marine algae (seaweeds) associated with coral reefs in the Gulf. In:

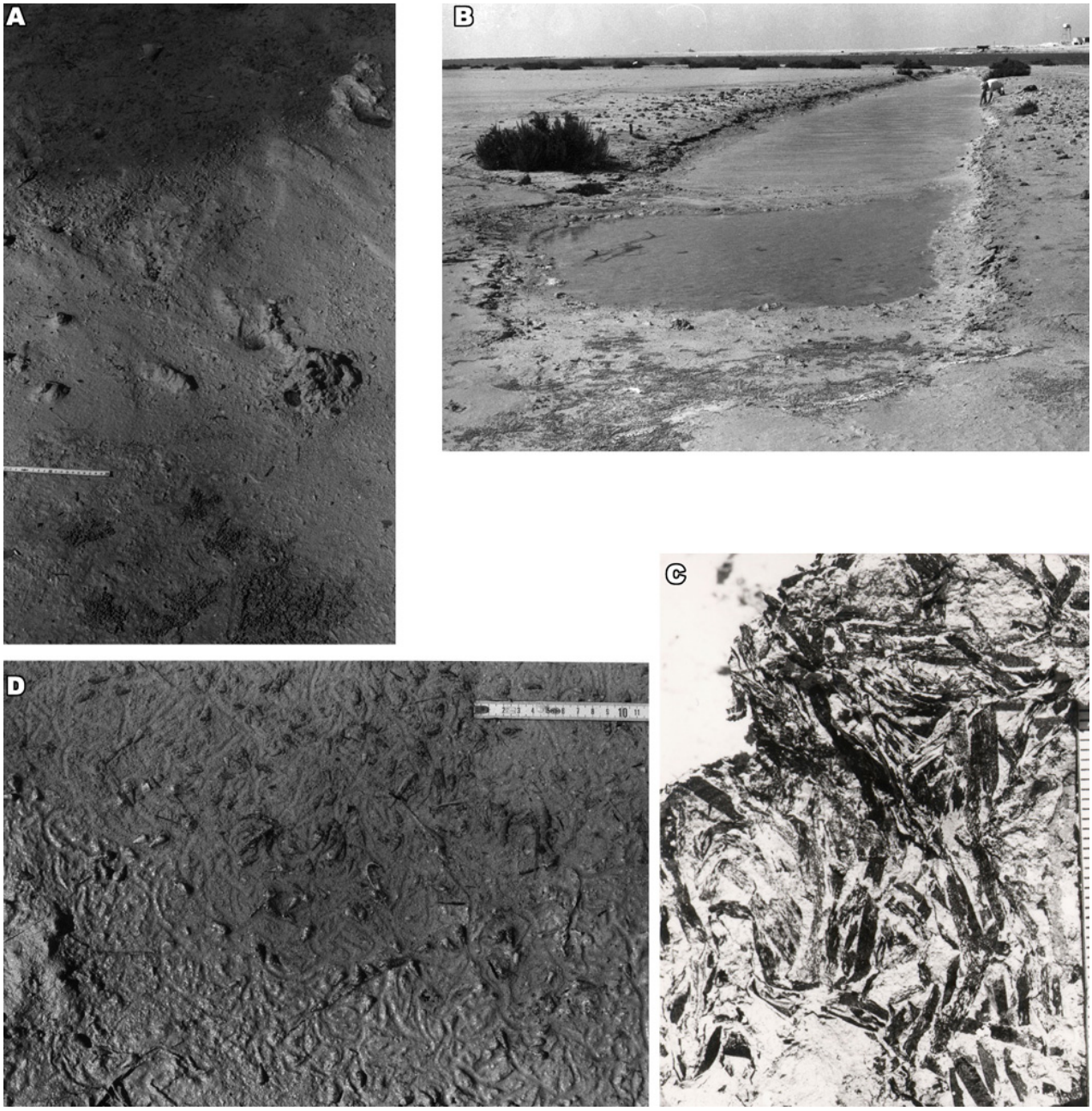

Figure 13: [by courtesy of Jean-Claude PLAZIAT, Mussafah, February 1987]**:** A) the upper part is a puddle of water with living Potamids; the middle part is a zone with crab burrows; the lower part is a zone with sand pellets made by "sand bubbler crabs", *Scopimera* spp.; **B)** a small channel with Potamids on the side of Mussafah channel. At low tide, it is disconnected from the main channel; **C)** detail of the zone with living Potamids; **D)** a layer made of drift seagrass leaves found in the mud below the upper microbial mat (Fig. 9.A).

RIEGL B.M. & PURKIS S.J. (eds.), Coral Reefs of the Gulf.- *Coral Reefs of the World*, vol. 3, p. 309-335.

KASSLER P. (1973).- The structural and geomorphologic evolution of the Persian Gulf. *In*: PURSER B.H. (ed.), The Persian Gulf.- Springer Verlag, Berlin, p. 11-32.

KENDALL C.G.St.C. & SKIPWITH P.A. d'E. (1969a).- Holocene shallow-water carbonate and evaporite sediments of Khor al Bazam, Abu Dhabi, South-West Persian Gulf.- *American Association of Petroleum Geologists*, *Bulletin*, vol. 53, no. 4, p. 841-869.

KENDALL C.G.St.C. & SKIPWITH P.A. d'E. (1969b).- Geormorphology of a recent shallow-water carbonate province Khor al Bazam, Trucial Coast, Southwest Persian Gulf.- *Geological Society of America*, *Bulletin*, vol. 80, no. 5, p. 865-892.

KENIG F. (1991).- Sédimentation, distribution et diagénèse de la matière organique dans un environnement carbonaté hypersalin, le système lagune-sabkha d'Abu Dhabi (É.A.U.).- Thèse de l'Université d'Orléans, 330 p.

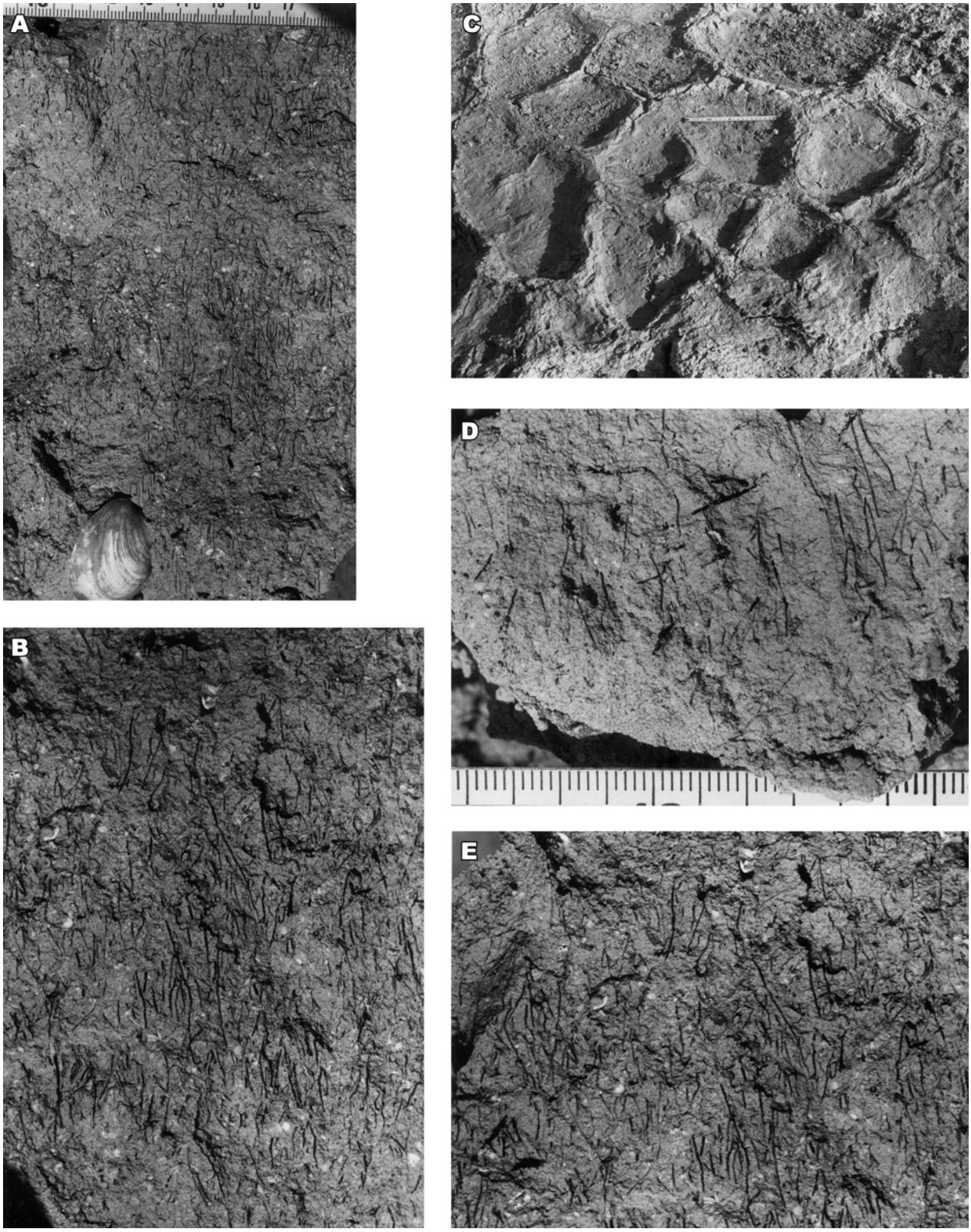

Figure 14: [by courtesy of Jean-Claude PLAZIAT, Mussafah, February 1987]**: A-B & D-E)** the muddy seagrass meadow facies with roots and a few rhizomes. In A, the pelecypod *Anodontia edentula* (LINNAEUS, 1758); **C)** polygonal pattern after ? desiccation cracks of the upper microbial mat.

KENIG F. (2011).- Distribution of organic matter in the transgressive and regressive Holocene sabkha sediments of Abu Dhabi, United Arab Emirates.- *International Association of Sedimentology*, *Special Publication*, vol. 43, p. 277-298.

KENIG F., HUC A.Y., PURSER B.H. & OUDIN J.-L. (1990).- Sedimentation, distribution and diagenesis of organic matter in a recent carbonate environment, Abu Dhabi, U.A.E.- *Organic Geochemistry*, vol. 16, no. 4-6, p. 735-747.

KINSMAN D.J.J. (1964).- The recent carbonate sediment near Halat El Bahrani, Trucial Coast, Persian Gulf. *In*: STRAATEN L.M.J.U. van (ed.), Deltaic and shallow marine deposits.- 6th International Sedimentological Congress, 1963.- *Developments in Sedimentology*, Elsevier, Amsterdam, vol. 1, p. 185-192.

KINSMAN D.J.J. (1971).- Early diagenesis of carbonate sediments in a supratidal evaporite setting.- *American Association of Petroleum Geologists*, *Bulletin*, vol. 55, no. 1, p. 167-168.

LAMBECK K. (1996).- Shoreline reconstructions for the Persian Gulf since the last glacial maximum.- *Earth and Planetary Science Letters*, vol. 142, p. 43-57.

MCKENZIE J.A. (1981).- Holocene dolomitization of calcium carbonate sediments from the coastal sabkhas of Abu Dhabi, U.A.E. A stable isotope study.- *Journal of Geology*, Chicago, vol. 89, p. 185-198.

MONTY C.L.V. (1973).- Remarques sur la nature, la morphologie et la distribution spatiale des stromatolithes. *In*: Sédimentation et diagénèse des carbonates actuels.- *Sciences de la Terre*, Nancy, vol. 18, no. 3, p. 191-212.

MURRAY J.W. (1966).- The foraminifera of the Persian Gulf. 3. The Halat al Bahrani region.- *Palæogeography, Palæoclimatology, Palæoecology*, vol. 2, p. 59-68.

MURRAY J.W. (1970).- The foraminifera of the hypersaline Abu Dhabi lagoon, Persian Gulf.- *Lethaia*, vol. 3, no. 1, p. 51-68.

STROHMENGER C.J., AL-MANSOORI A., AL-JEELANI O., AL-SHAMRY A., AL-HOSANI I., AL-MEHSIN K. & SHEBL H. (2010).- The sabkha sequence at Mussafah Channel (Abu Dhabi, United Arab Emirates): facies stacking patterns, microbial-mediated dolomite and evaporite overprint.- *GeoArabia*, vol. 15, no. 1, p. 49-90.

PATTERSON R.J. & KINSMAN D.J.J. (1982).- Formation of diagenetic dolomite in coastal sabkha along Arabian (Persian) Gulf.- *American Association of Petroleum Geologists*, *Bulletin*, vol. 66, no. 1, p. 28-43.

PLAZIAT J.-C. (1993).- Modern and fossil Potamids (Gastropoda) in saline lakes.- *Journal of Paleolimnology*, vol. 8, no. 2, p. 163-169.

PURSER B.H. & EVANS G. (1973).- Regional sedimentation along the Trucial Coast, SE Persian Gulf. *In*: PURSER B.H. (ed.), The Persian Gulf.- Springer Verlag, Berlin, p. 211-231.

REINECK H.E. & SINGH I.B. (1973).- Depositional sedimentary environments.- Springer Verlag, Berlin, 439 p.

RIOULT M. & DANGEARD L. (1976).- Importance des Cryptogames perforantes marines en géologie. *In*: Travaux de biologie végétale dédiés au Professeur P. DANGEARD.- *Le Botaniste*, Caen, (L), p. 389-413.

SHEARMAN D.J. (1966).- Origin of marine evaporite by diagenesis.- *Transactions of the Institution of Mining and Metallurgy*, London, (B), vol. 75, p. 207-215.

TRICHET J. (1967).- Essai d'explication du dépôt d'aragonite sur des substrats organiques.- *Comptes Rendus de l'Académie des Sciences de Paris*, t. 265, (D), p. 1464-1467.

WAGNER C.W. & TOGT C. van der (1973).- Holocene sediment types and their distribution in the southern Persian Gulf. *In*: PURSER B.H. (ed.), The Persian Gulf.- Springer Verlag, Berlin, p. 123-155.

Plates

Plate 1: *Acetabularia*

Figs. 1-2: Calcified cap of an *Acetabularia* sp. viewed from above. The scars of the fertile ampulae are visible on these caps;
Fig. 3: Calcified cap of an *Acetabularia* sp. viewed from the side. The scars of the fertile ampulae are visible on the upper corona structure whereas the lower corona structure is well-preserved. Below the cap, along the calcareous coating of the thallus, scars arranged in a whorl correspond to the bases of sessile sterile laterals;
Fig. 4: These three broken specimens of *Acetabularia* sp. document the measurement variations between discrete specimens within the same species (a and c) as well as those observed within a single specimen (b);
Fig. 5: To the left, tangential section of an *Acetabularia* cap with some pores (arrows) connecting the thallus cavity and the corona structure at the base of the fertile ampulae. To the right, oblique section of an *Acetabularia* thallus that displays discrete layers within its aragonitic coating. The feature that favoured the coating breakage (arrow) is visible in very few specimens. Sample ABA 175, 4.2 km - J;
Fig. 6: Detail of figure 7. Several microstructures are visible on the outer surface of the thallus calcareous. Some correspond to selective dissolution of the aragonitic cortex, *i.e.*, dissolution microcraters and crests related to cryptogamic and microbial borings (small arrows) and others to calcified coccoid structures (large arrows);
Fig. 7: Calcified anchoring organ of an *Acetabularia* thallus.

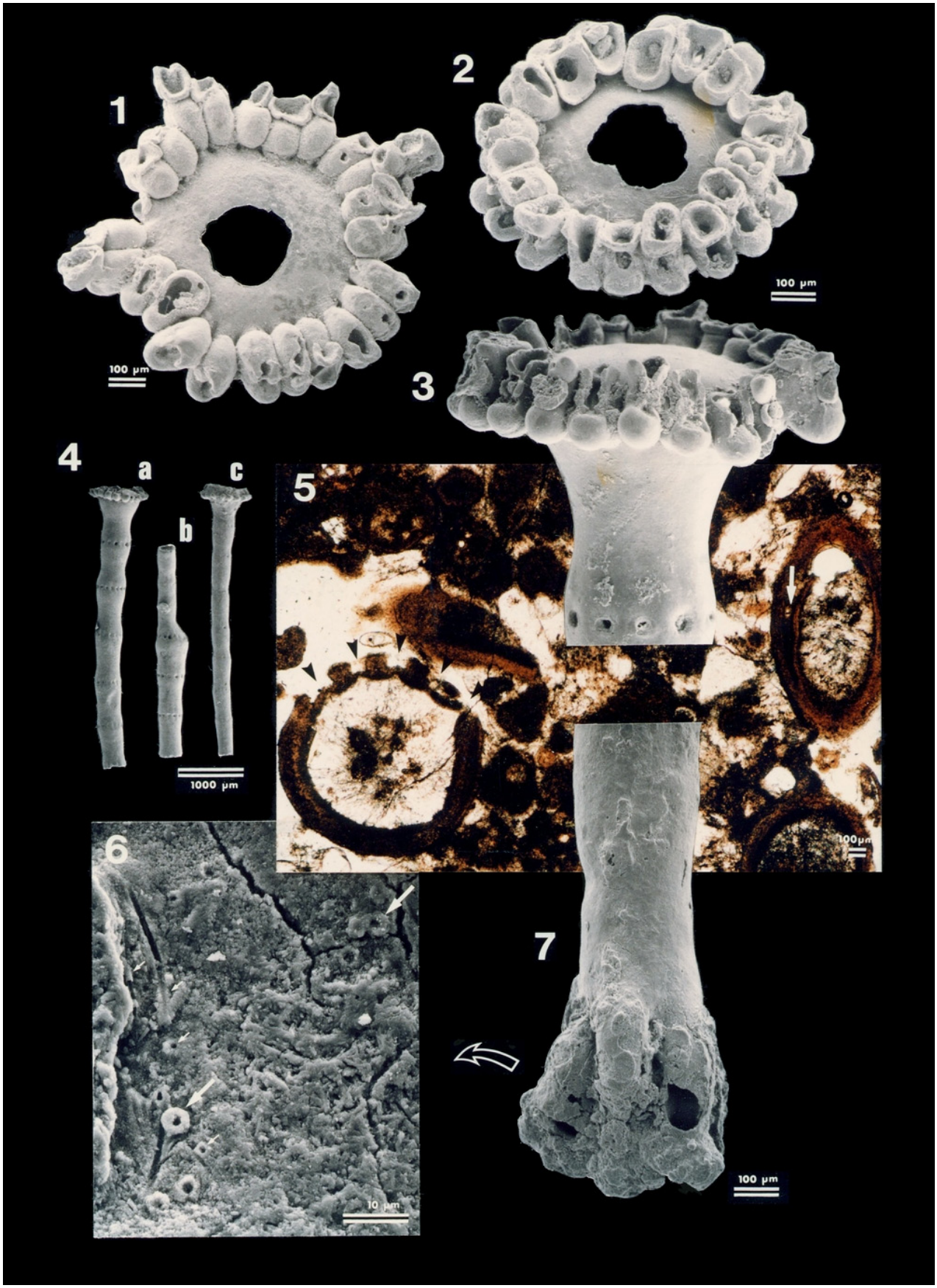
1
100 µm
2
100 µm
3
4
a
b
c
1000 µm
5
100µm
6
10 µm
7
100 µm

Plate 2: *Spirorbis*

Fig. 1: Axial section of a *Spirorbis* tube. Sample ABA 172, 6 km - G;
Fig. 2: Oblique section of a *Spirorbis* tube. Sample ABA 172, 6 km - G;
Fig. 3: Section of annelid tubes with a free encrusting basal surface molding a formerly rigid, non-fossilized support. Senegal, Well Br 1, Core 32, Box 3, Lower Cretaceous;
Fig. 4: The most common form of bryozoans found in the area;
Fig. 5: Encrusting basal surface of a *Spirorbis* tube. On the right side the vertical imprint corresponds to a relief structure on the formerly rigid, non-fossilized support;
Fig. 6: The tube of this *Spirorbis* specimen, the opening of which is visible, has longitudinal crests and transverse grooves on its outer side;
Fig. 7: *Spirorbis* tubes on an *Acetabularia* thallus.


1
500 µm
2
500 µm
3
250 µm
4
250 µm
5
250 µm
6
250 µm
7
100 µm

Plate 3: *Spirorbis* and Diatoms

Fig. 1: Encrusting basal surface of a *Spirorbis* tube molding its non-fossilized support, a large piece either of seaweed or of seagrass;
Fig. 2: Detail of figure 1 with the imprint of a diatom frustule;
Fig. 3: Diatom frustule, replaced by calcite, on the encrusting basal surface of a *Spirorbis* tube;
Fig. 4: Detail of the imprint of a diatom frustule visible on figure 2;
Fig. 5: Imprint of another diatom frustule on the encrusting basal surface of a *Spirorbis* tube;
Fig. 6: Encrusting basal surface of a *Spirorbis* group;
Fig. 7: Diatom frustules replaced by calcite and various imprints visible on the encrusting basal surface of a *Spirorbis* tube.

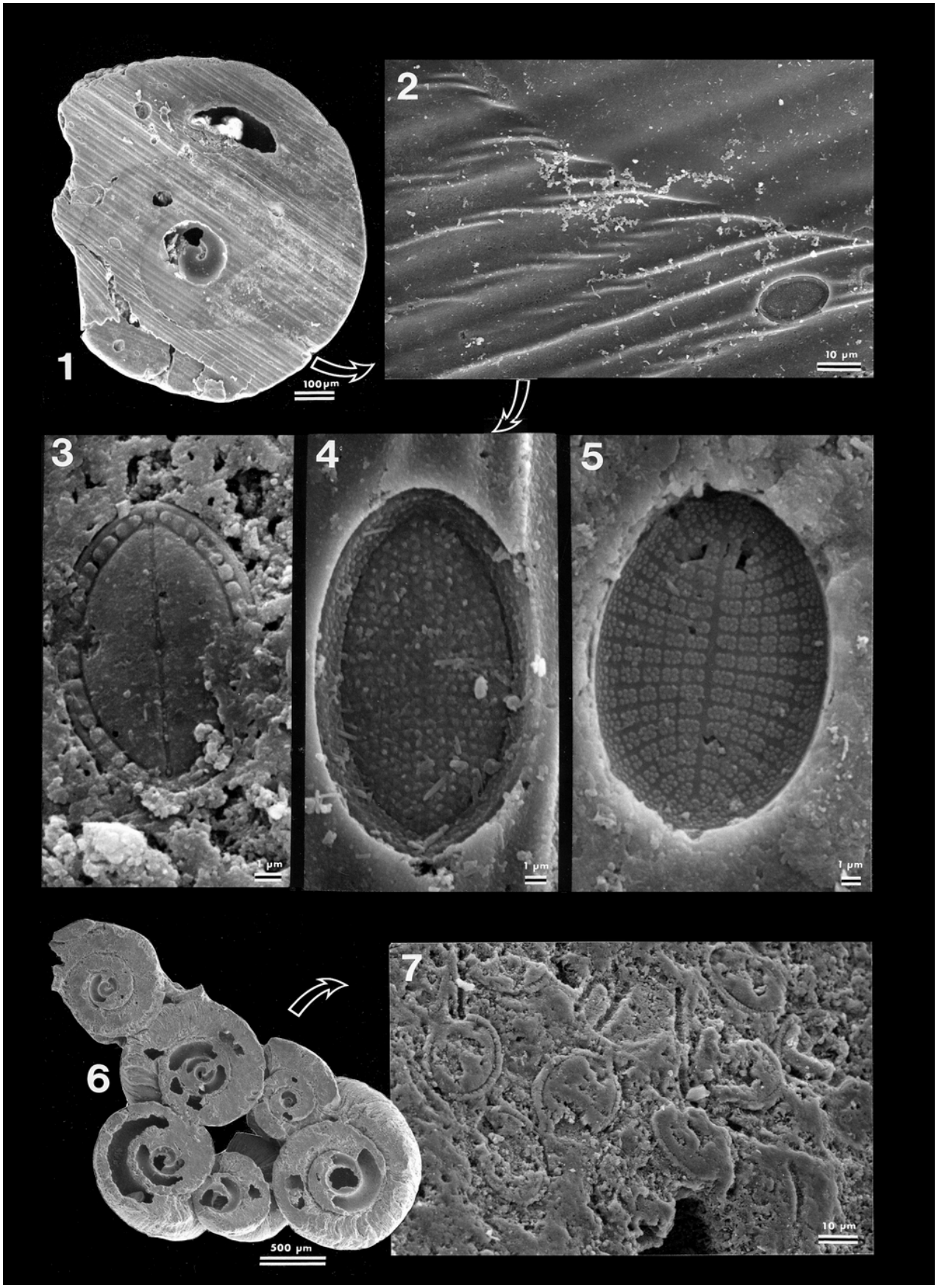
1
100 µm
2
10 µm
3
1 µm
4
1 µm
5
1 µm
6
500 µm
7
10 µm

Plate 4: *Spirorbis* and Rhodophyta (Photos Hermes BRITO, UNESPEtro)

Fig. 1: Encrusting basal surface of a *Spirorbis* tube molding encrusting Rhodophyta;
Fig. 2: Detail of figure 1 with the imprint of diatom frustules (yellow arrows);
Fig. 3: Encrusting basal surface of a *Spirorbis* tube molding encrusting Rhodophyta, probably a *Lithophyllum*;
Fig. 4: Detail of the Rhodophyta.

[All scales represent 100 µm]

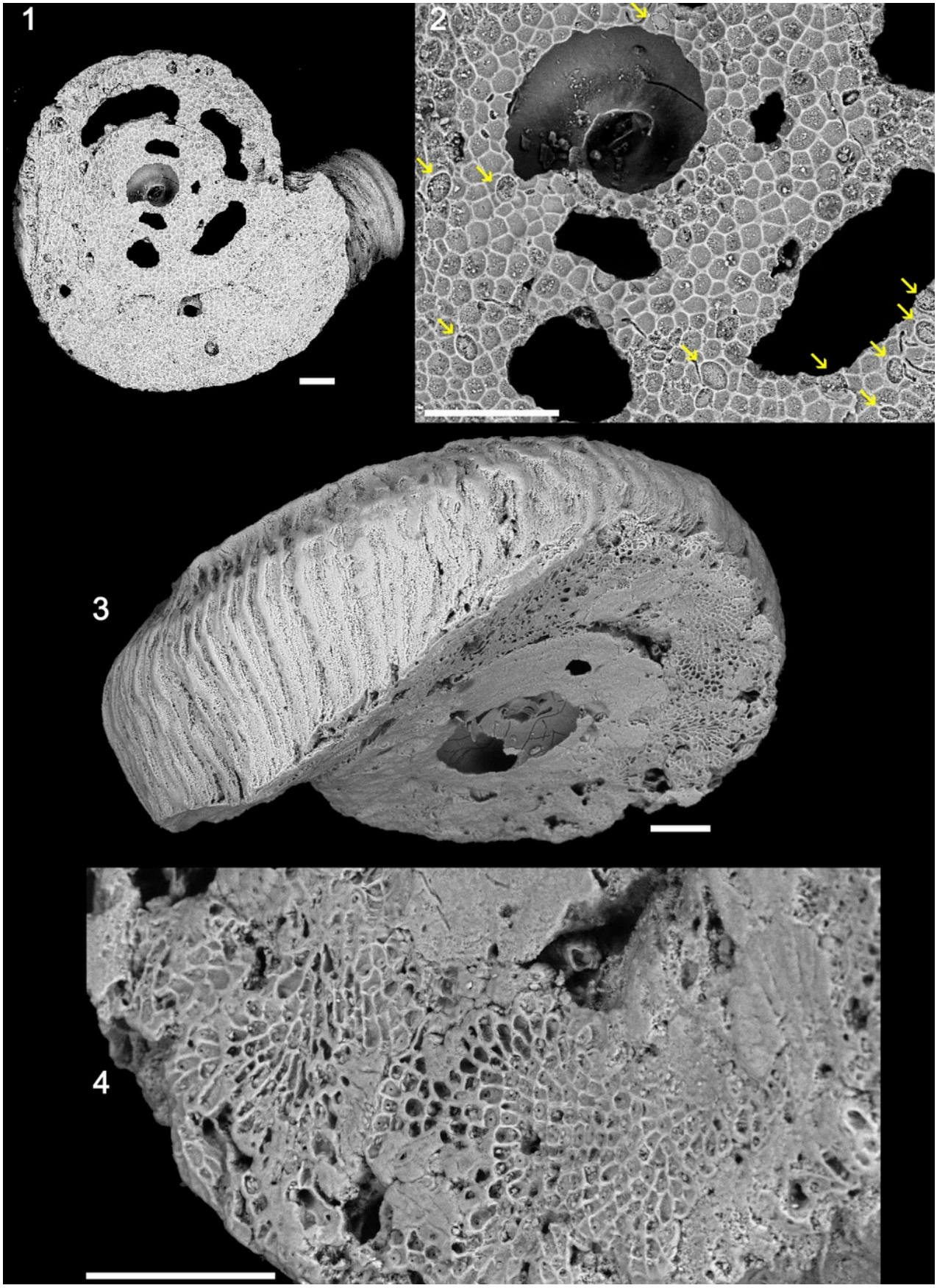
1
2
3
4

Plate 5: Ostracods and small benthic Foraminifers

Figs. 1-2: *Gibboborchella* sp. 1) left valve; 2) dorsal view.
Figs. 3-4: ? *Cistacythereis* sp. 3) right valve; 4) dorsal view.
Figs. 5-6: *Alocopocythere reticulata indoaustralica* HARTMANN, 1978. 5) left valve; 6) dorsal view.
Figs. 7-9: *Elphidium striatopunctatum* (FICHTEL & MOLL, 1798). 7) apertural view; 8) lateral view; 9) profile view;
Figs. 10-14: *Ammonia convexa* (COLLINS, 1958). 10) dorsal view; 11) apertural view; 12) oblique ventral view; 13) dorsal view; 14) ventral view.

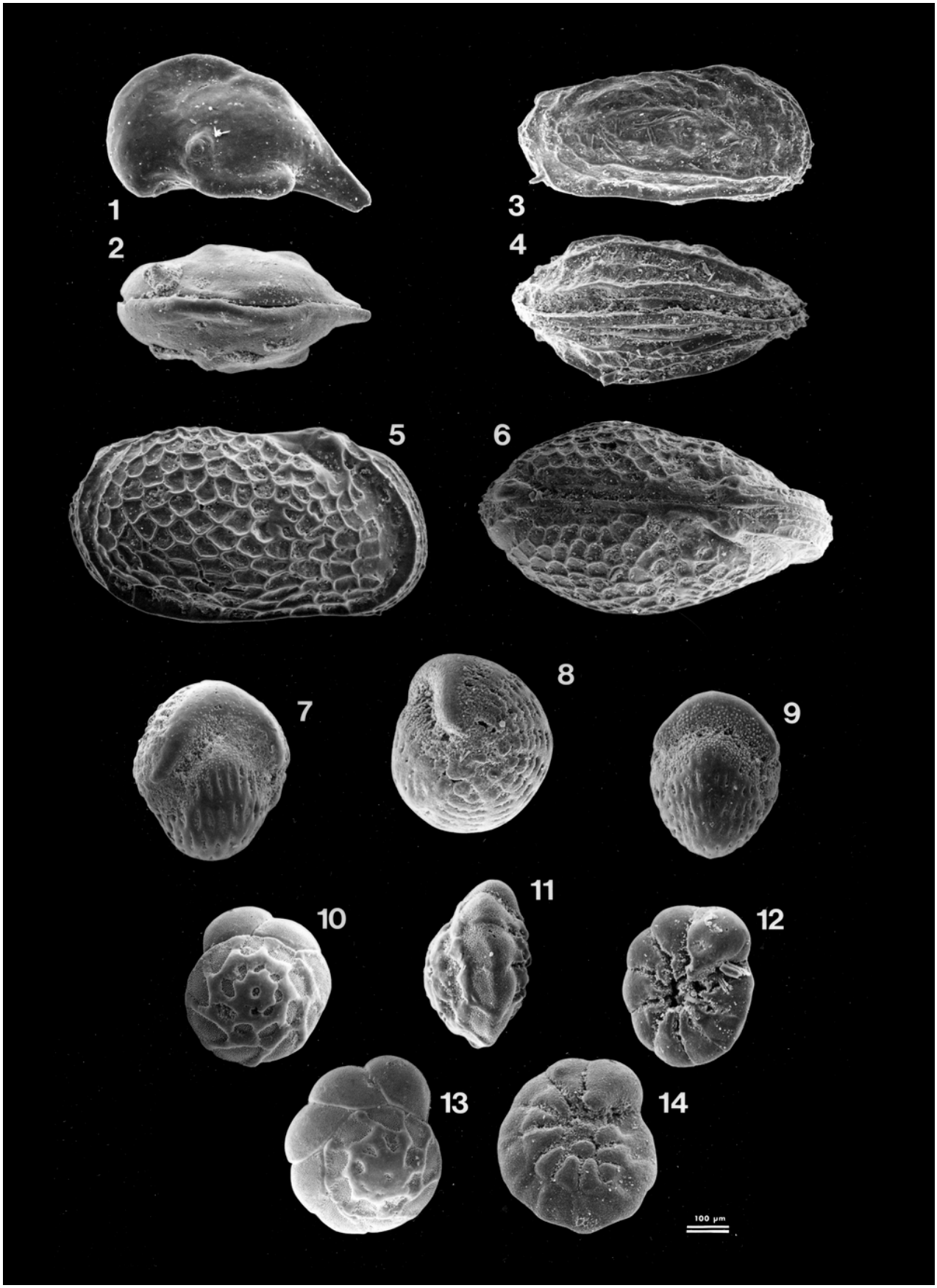
1
2
3
4
5
6
7
8
9
10
11
12
13
14
100 µm

Plate 6: Foraminifers

Fig. 1: *Elphidium* sp., equatorial section. Sample ABA 171, 4.2 km - G;
Fig. 2: *Elphidium* sp., axial section. Sample ABA 174, 4.2 km - I;
Fig. 3: *Elphidium* sp., subequatorial section. Sample ABA 174, 4.2 km - I;
Fig. 4: *Monalysidium acicularis* (BATSCH, 1791), and regular and aberrant forms of *Peneroplis planatus* (FICHTEL & MOLL, 1798);
Fig. 5: *Peneroplis* sp., tangential section. Sample ABA 166, 0,6 km - F.
Fig. 6: *Ammonia* sp., oblique section. Sample ABA 171, 4.2 km - G;
Fig. 7: *Ammonia* sp., sub-axial section. Sample ABA 175, 4.2 km - J;
Fig. 8: *Peneroplis* sp., equatorial section. Sample ABA 167, 1.6 km - F.

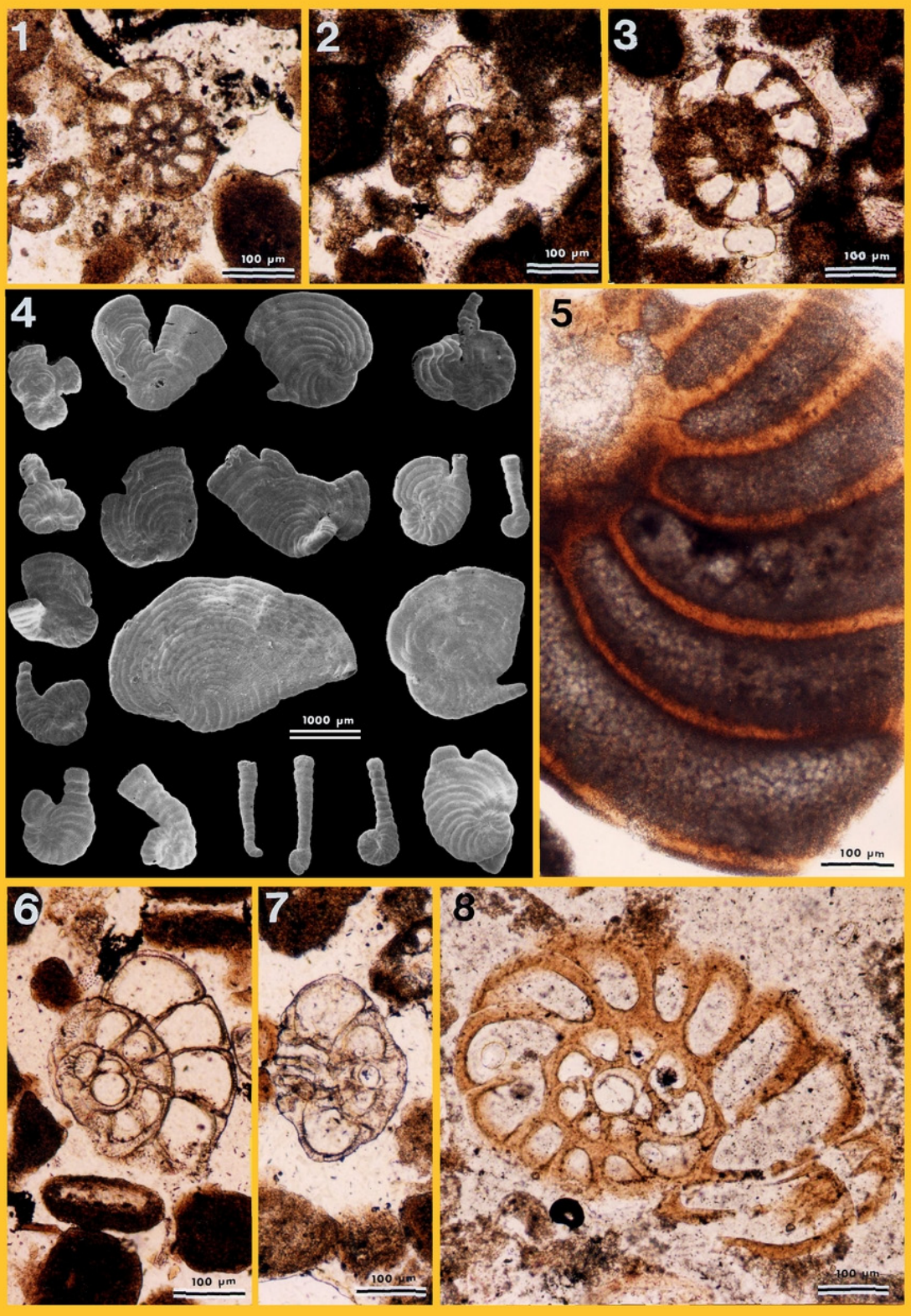
1
100 µm
2
100 µm
3
100 µm
4
1000 µm
5
100 µm
6
100 µm
7
100 µm
8
100 µm

Plate 7: Foraminifers: Miliolidae

Fig. 1: Encrusted and bored test of a *Quinqueloculina* sp., morphological type B of MURRAY, 1966;
Fig. 2: *Miliammina fusca* (BRADY, 1870). The agglutinate consists of various small bioclasts, *e.g.*, microforaminifers (figure 3) and coccoliths (figure 4);
Fig. 3: Detail of figure 2, a microforaminifer in the agglutinate of *Miliammina fusca* (BRADY, 1870);
Fig. 4: Detail of figure 2, a coccolith in the agglutinate of *Miliammina fusca* (BRADY, 1870);
Fig. 5: *Miliammina fusca* (BRADY, 1870);
Fig. 6: *Quinqueloculina* sp., morphological type B of MURRAY, 1966;
Fig. 7: *Quinqueloculina* sp., morphological type B of MURRAY, 1966;
Fig. 8: *Spiroloculina angulata* CUSHMAN, 1917;
Fig. 9: *Quinqueloculina* sp., morphological type B of MURRAY, 1966;
Fig. 10: *Quinqueloculina* sp., morphological type F of MURRAY, 1966;
Fig. 11: *Quinqueloculina* sp., morphological type F of MURRAY, 1966;
Fig. 12: *Spiroloculina angulata* CUSHMAN, 1917.

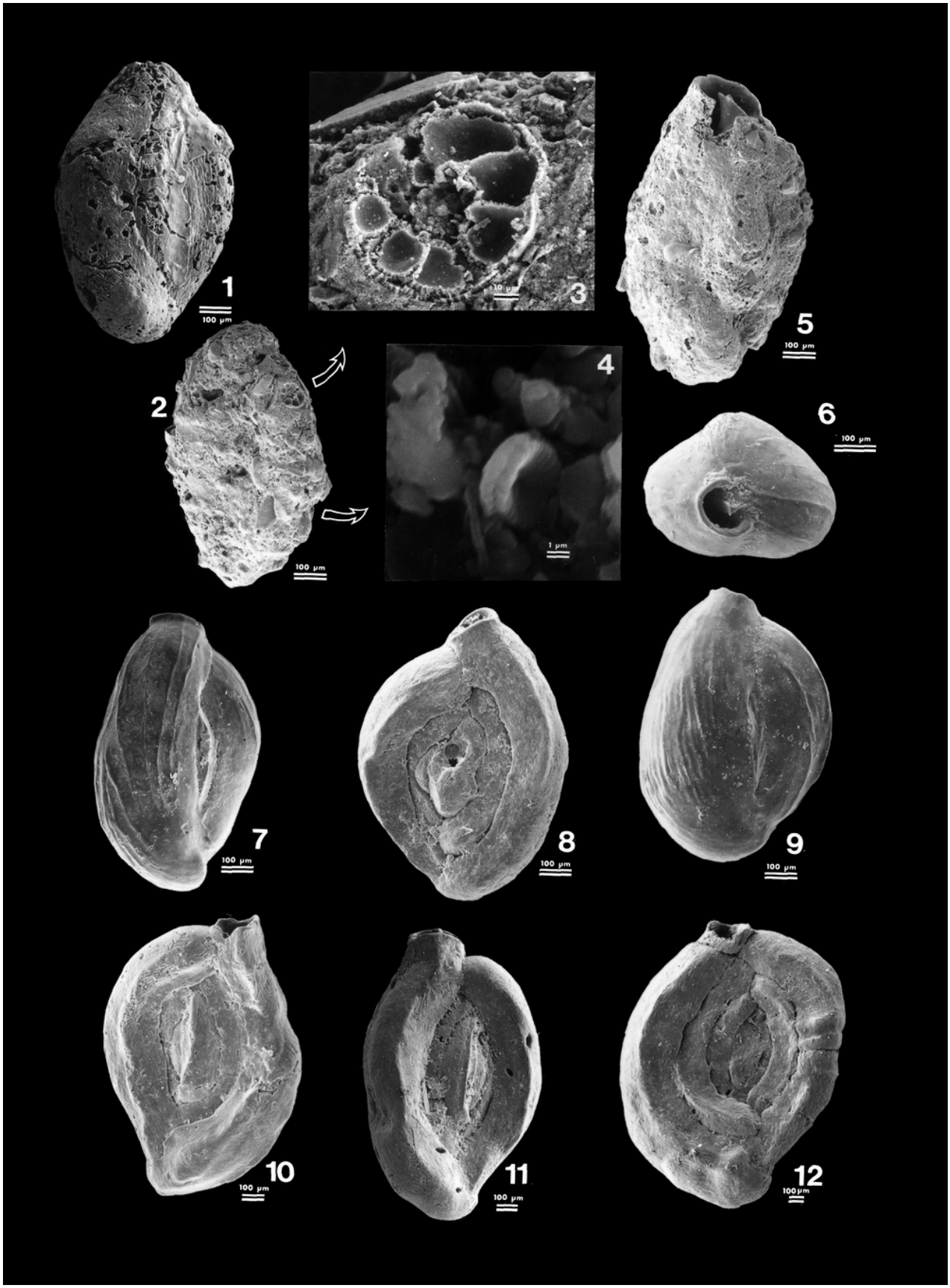
1
100 µm
2
100 µm
3
10 µm
4
1 µm
5
100 µm
6
100 µm
7
100 µm
8
100 µm
9
100 µm
10
100 µm
11
100 µm
12
100 µm

Plate 8: Foraminifers and faecal pellets

Fig. 1: *Sorites orbiculus* (FORSKAL, 1775);
Fig. 2: *Sorites orbiculus* (FORSKAL, 1775);
Fig. 3: *Peneroplis planatus* (FICHTEL & MOLL, 1798);
Fig. 4: *Peneroplis planatus* (FICHTEL & MOLL, 1798);
Fig. 5: Faecal pellets with a spiral structure;
Fig. 6: Diatom frustule in a faecal pellet. Dolomite rhombs are present within the surrounding mesh made of aragonitic needles.

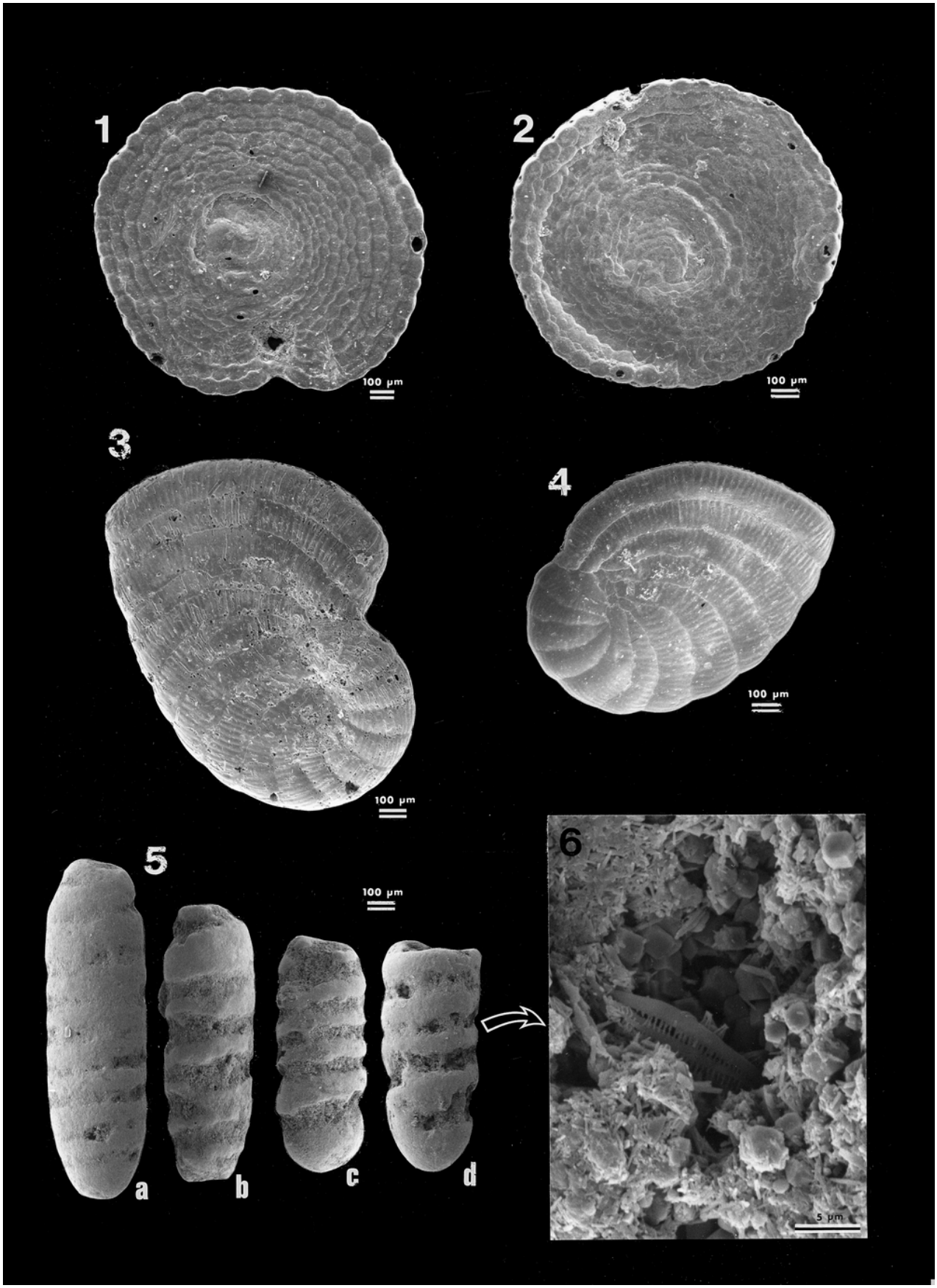
1
100 µm
2
100 µm
3
100 µm
4
100 µm
5
100 µm
a
b
c
d
6
5 µm

Plate 9: Extraclasts

Fig. 1: To the left, the subaxial section of an agglutinated Textulariid test represents the main part of an extraclast found in the basal holocene Potamid beach-rock; to the right, the honey-colored section of foraminifer is ascribed to a *Peneroplis* sp. Sample ABA 167, 1.6 km - F;
Fig. 2: Subequatorial section of an agglutinated Lituolid test in an extraclast found in the Pleistocene sands. Sample ABA 96, 14 B - IV;
Fig. 3: Subaxial section of an agglutinated Textulariid test in an extraclast found in the Pleistocene sands. Sample ABA 104, 14 D - V;
Fig. 4: This subaxial section of an agglutinated Textulariid test represents two thirds of an extraclast found in the Pleistocene sands. The apical part of the test and the calcitic cement within the foraminifer chambers show evidence of mechanical abrasion. Sample ABA 170, 0 km - G;
Fig. 5: Axial section of a Lenticulina sp., probably part of an extraclast found in the Pleistocene sands. Sample ABA 170, 0 km - G;
Fig. 6: Subequatorial section of a *Lenticulina* sp. with micritic fills in its chambers found in a Holocene anhydritic layer. The outer part of the test shows evidence of mechanical abrasion. Sample ABA 124, 1.6 km - A.

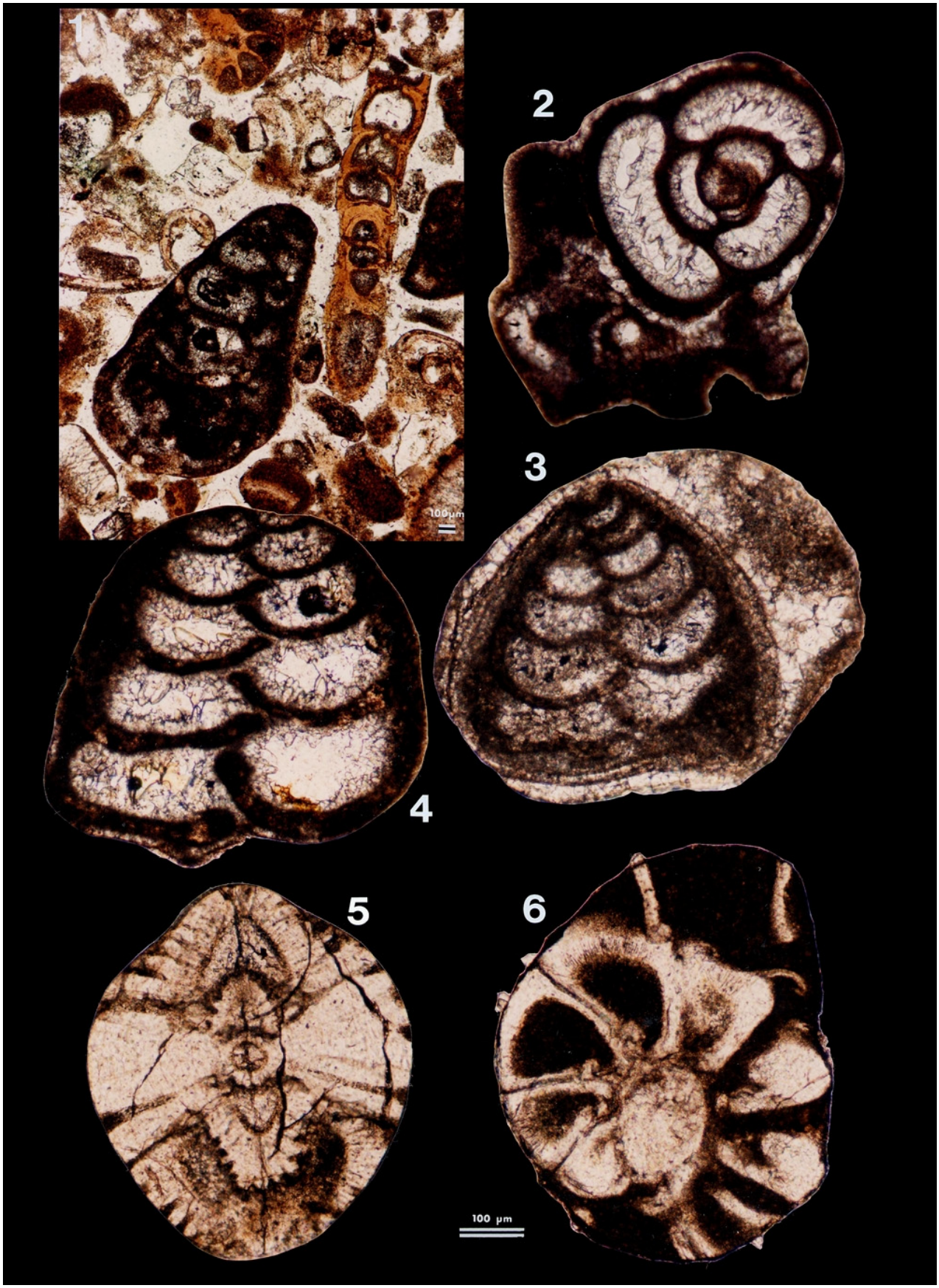
1
100µm
2
3
4
5
6
100 µm

Plate 10: Extraclasts

Fig. 1: This extraclast, *i.e.*, a lithoclast found in the Pleistocene sands, is made of calcitic ooids mostly bonded by clotted micrite. Sample ABA 104, 14 D - V;
Fig. 2: Calcitic ooid found in the Holocene anhydritic layer (? aeolian sands). Sample ABA 124, 1.6 km - A;
Fig. 3: Aragonitic ooid from a sampling at the modern beach in Abu Dhabi. Borings resulting from the activity of several types of organisms, including microbes, are common. Sample ABA 120, Le Méridien (hotel), Abu Dhabi;
Fig. 4: Calcitic ooid found in the Holocene anhydritic layer (? aeolian sands). It consists mostly of calcite sparite with a mosaic pattern. Few concentric micritic layers are still preserved. Sample ABA 124, 1.6 km - A;
Fig. 5: Calcitic ooid found in the Holocene anhydritic layer. Sample ABA 124, 1.6 km - A;
Fig. 6: Section of a geniculate corallinale found in the Holocene anhydritic layer. Sample ABA 124, 1.6 km - A;
Fig. 7: Calcitic ooid found in the Holocene anhydritic layer. In place of the ooid nucleus there is a secondary drusy calcitic sparite indicative of dissolution of the primary aragonitic nucleus. Sample ABA 124, 1.6 km - A.

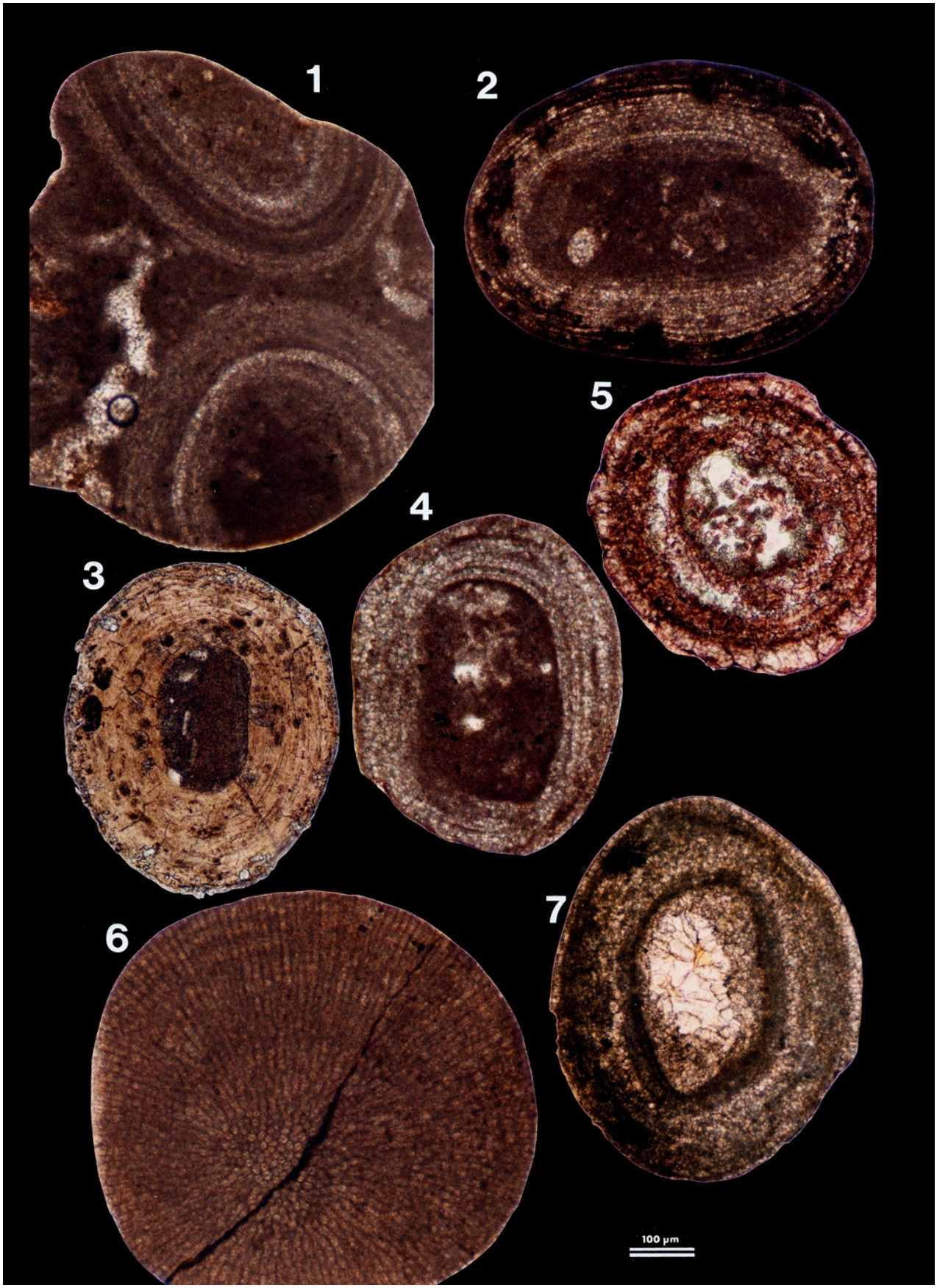
1
2
5
4
3
6
7
100 µm

Plate 11: Allochems

Fig. 1: Gastropod shell in the basal Potamid beach-rock. Fibrous cement has grown on the inner side of the shell. Structureless grains, *i.e.*, peloids, and grains with a fuzzy zoning, possible micritic ooids, are also found in the former body cavity. Sample ABA 145, 0,6 km - D;
Fig. 2: Because the surrounding grains are not truncated, this structure observed in the upper Potamid beach-rock can be interpreted either as a burrow or as a root mold. Sample ABA 174, 4.2 km - I;
Fig. 3: Microborings, either fungal or microbial, in a shell. The arrow points to a halo of corrosion surrounding a filament. Sample ABA 171, 4.2 km - G;
Fig. 4: This aggregate found in the Potamid sands consists of several micritic grains. The arrowed micritic ooid differs from the peloids due to its clear concentric structure. Sample ABA 171, 4.2 km - G;
Fig. 5: The arrowed micritic ooid is part of an aggregate found in the Potamid sands. The fringing aragonitic cement is weakly developed. Grains are mostly bonded by micritic bridges. Sample ABA 171, 4.2 km - G.

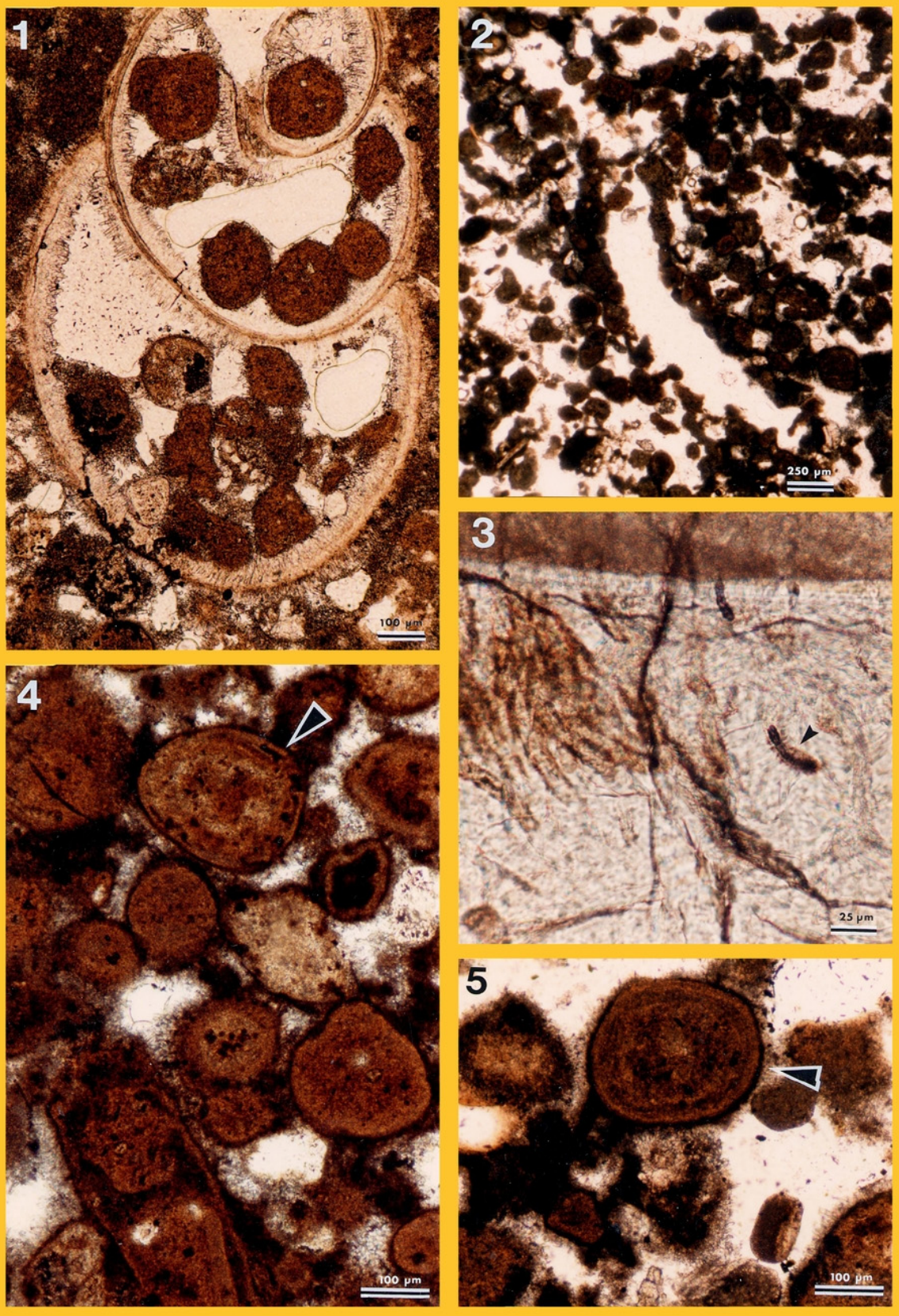
1
100 µm
2
250 µm
3
25 µm
4
100 µm
5
100 µm

Plate 12: Coccoids in a microbial mat

Figs. 1-3: Scattered or aggregated calcified coccoid structures in the lower microbial mat. Sample ABA 165, 0 km -F.

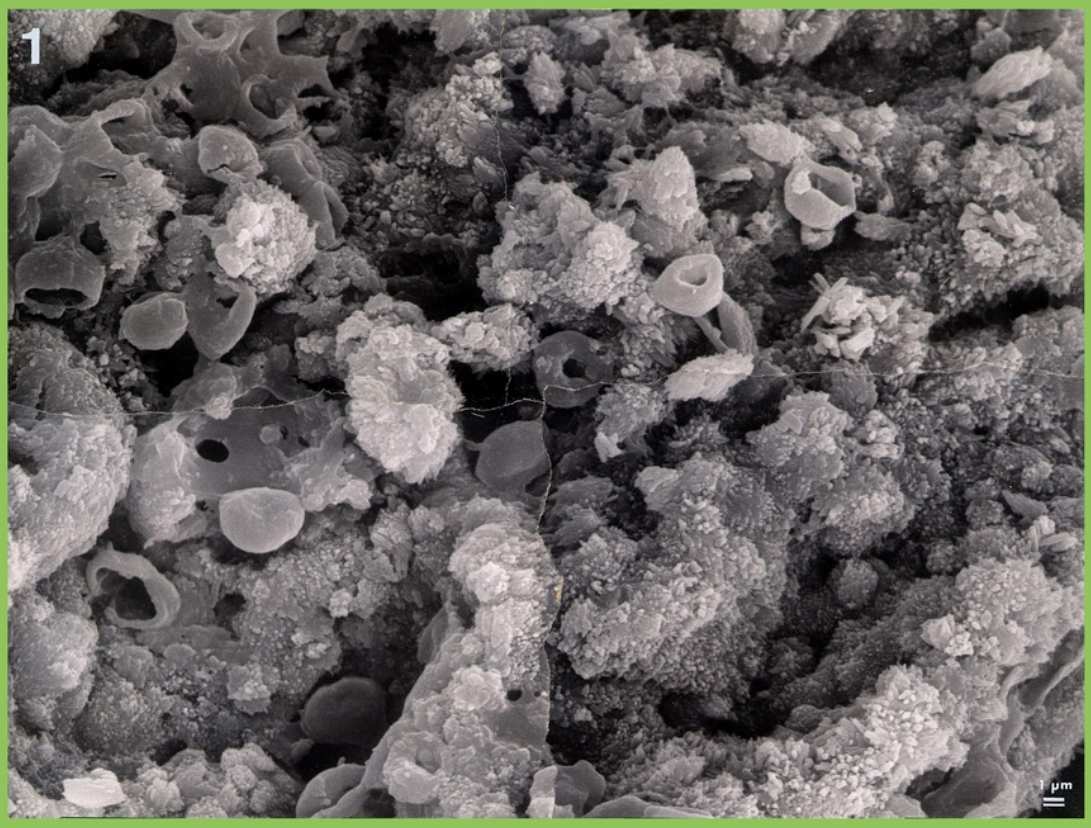
1
1 µm

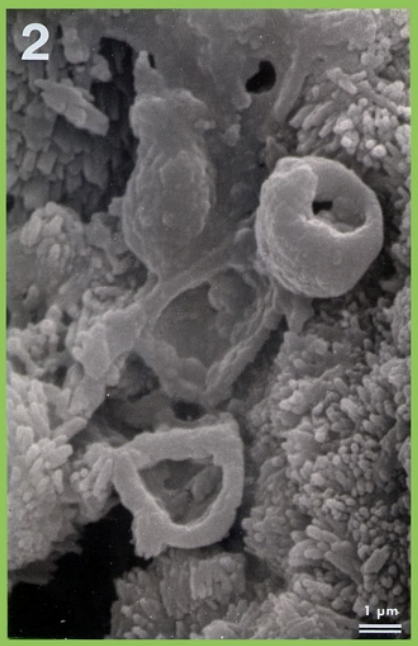
2
1 µm

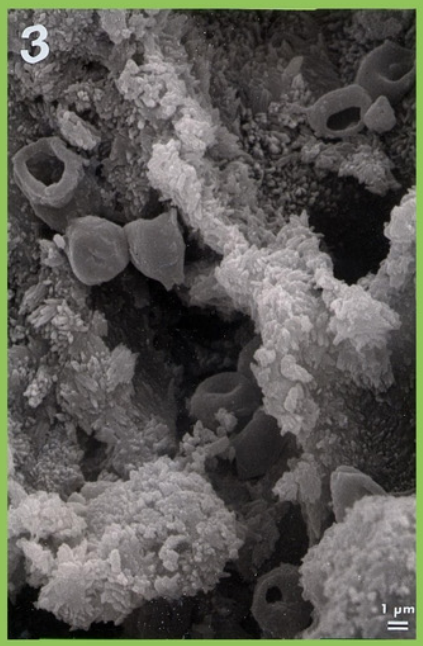
3
1 µm

Plate 13: Coccoids in a microbial mat

Fig. 1: Coccoids in the lower microbial mat. Scattered or aggregated calcified coccoid structures, in association with filamentous structures (arrows), are more or less easily discernible. Sample ABA 165, 0 km - F;
Figs. 2-5: Scattered or aggregated calcified coccoid structures in the lower microbial mat. Sample ABA 165, 0 km -F.

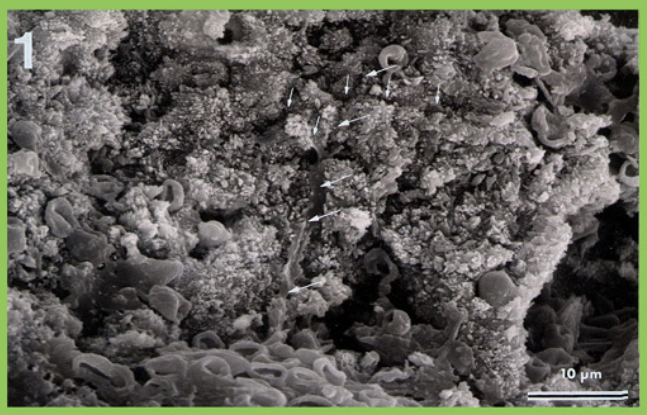
1
10 µm

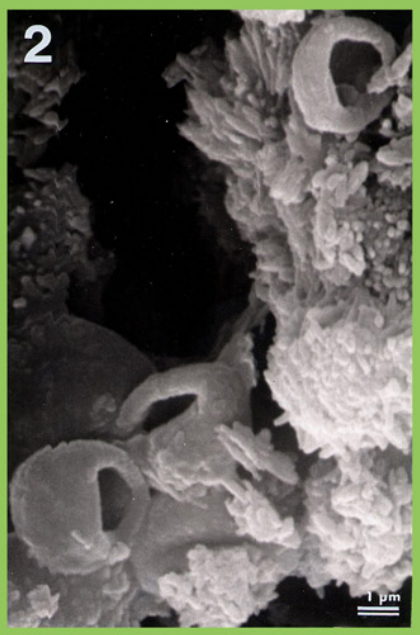
2
1 µm

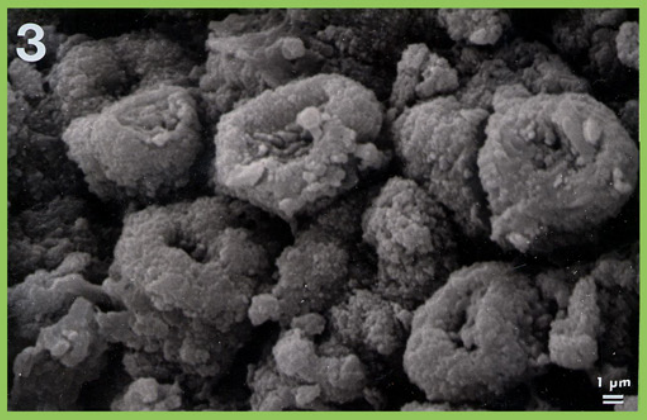
3
1 µm

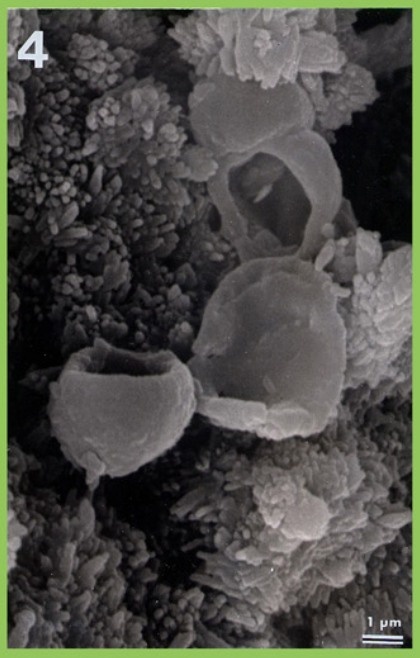
4
1 µm

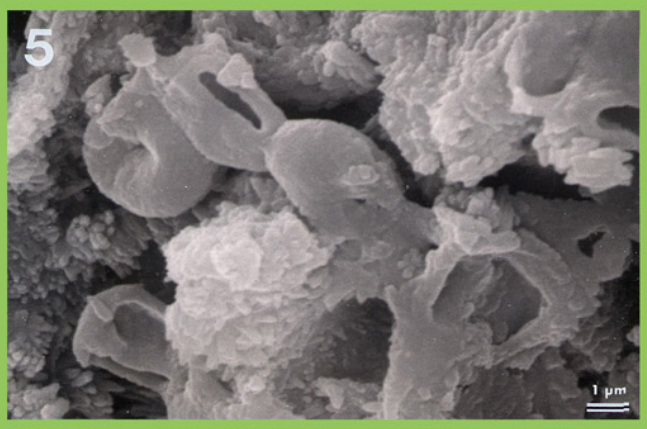
5
1 µm

Plate 14: *Miscellanea*

Fig. 1: A calcitic structure, probably a red alga, possibly *Bostrychia arbuscula* HARVEY, 1855, found in a mostly dolomitic intraclast of the lower microbial mat. Sample ABA 129, 2 km - A;
Fig. 2: A calcitic structure, probably a filamentous cyanobacteria, possibly *Coleofasciculus chthonoplastes* (GOMONT, 1892), found in a mostly dolomitic intraclast of the lower microbial mat. Sample ABA 129, 2 km - A;
Fig. 3: Same as in figure 2. Note the possible connection of two filaments (arrow);
Fig. 4: Isolated filament found in a mostly dolomitic intraclast of the lower microbial mat. Sample ABA 129, 2 km - A;
Fig. 5: Dolomite (? cement) in a lump. Sample ABA 176, 4.2 km - K;
Fig. 6: Detail of the mineralization of an *Acetabularia*'s thallus with a dense network of (? fungal or microbial) microborings extending from the outside of the calcareous coating;
Fig. 7: Fibrous cement from the upper Potamid beach-rock. Sample ABA 172, 6 km - G.

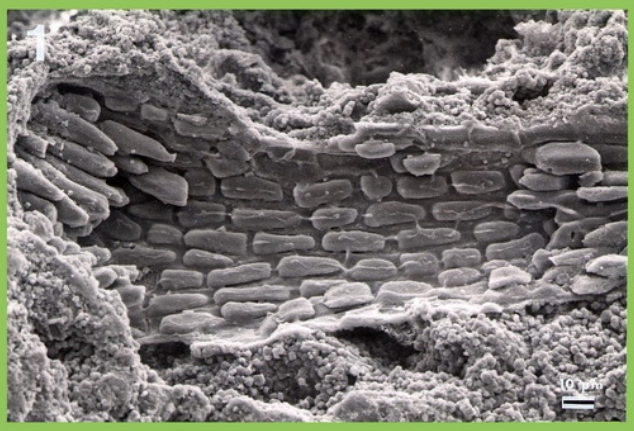
1
10 µm

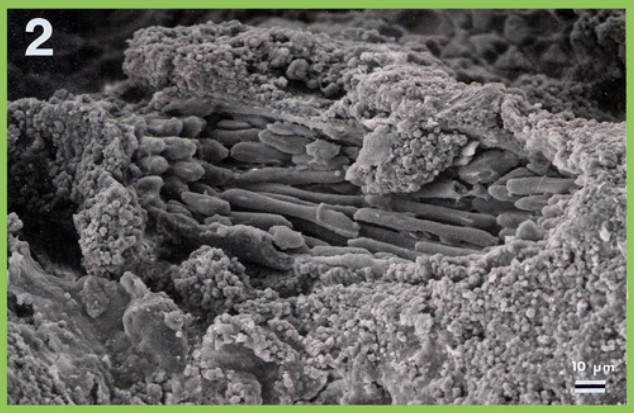
2
10 µm

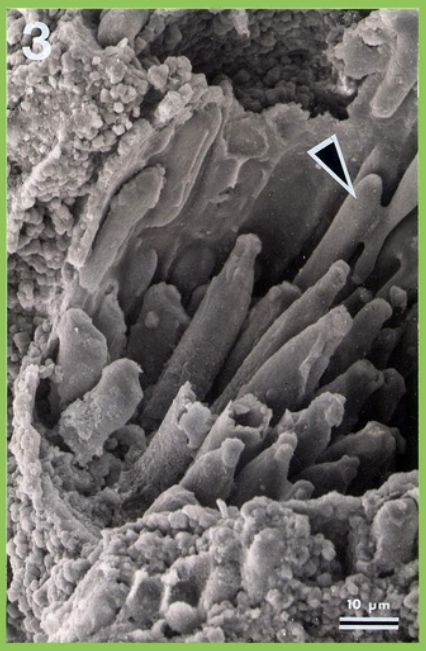
3
10 µm

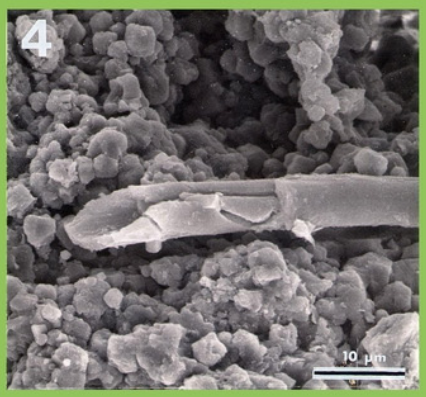
4
10 µm

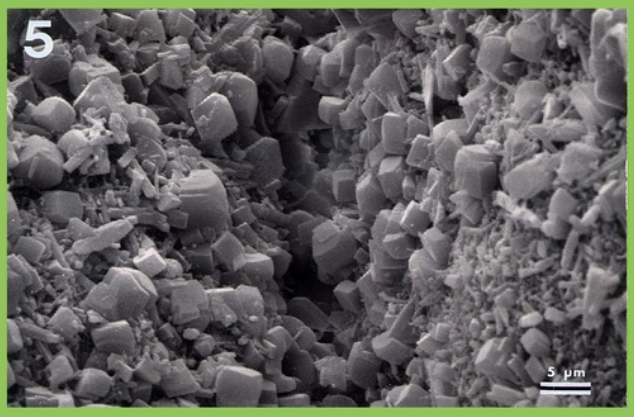
5
5 µm


6
1 µm


7
1 µm

Plate 15: Diagenesis

Fig. 1: "Rounded grain" with scattered calcite crystals (cement). Sample ABA 134, 4.2 km - B;
Fig. 2: Detail of some crystals of figure 1 documenting dissolution traces, *i.e.*, spiky calcite sensu FOLK et al. (1985). Sample ABA 134, 4.2 km - B;
Figs. 3-4: Calcite crystals with dissolution traces, *i.e.*, spiky calcite *sensu* FOLK et al. (1985). Sample ABA 134, 4.2 km - B;
Fig. 5: Aggregate of grains. Sample ABA 173, 4.2 km - H;
Fig. 6: Detail of figure 5 showing the arrangement of the fibrous cement on individual grains of this aggregate. Sample ABA 173, 4.2 km - H.

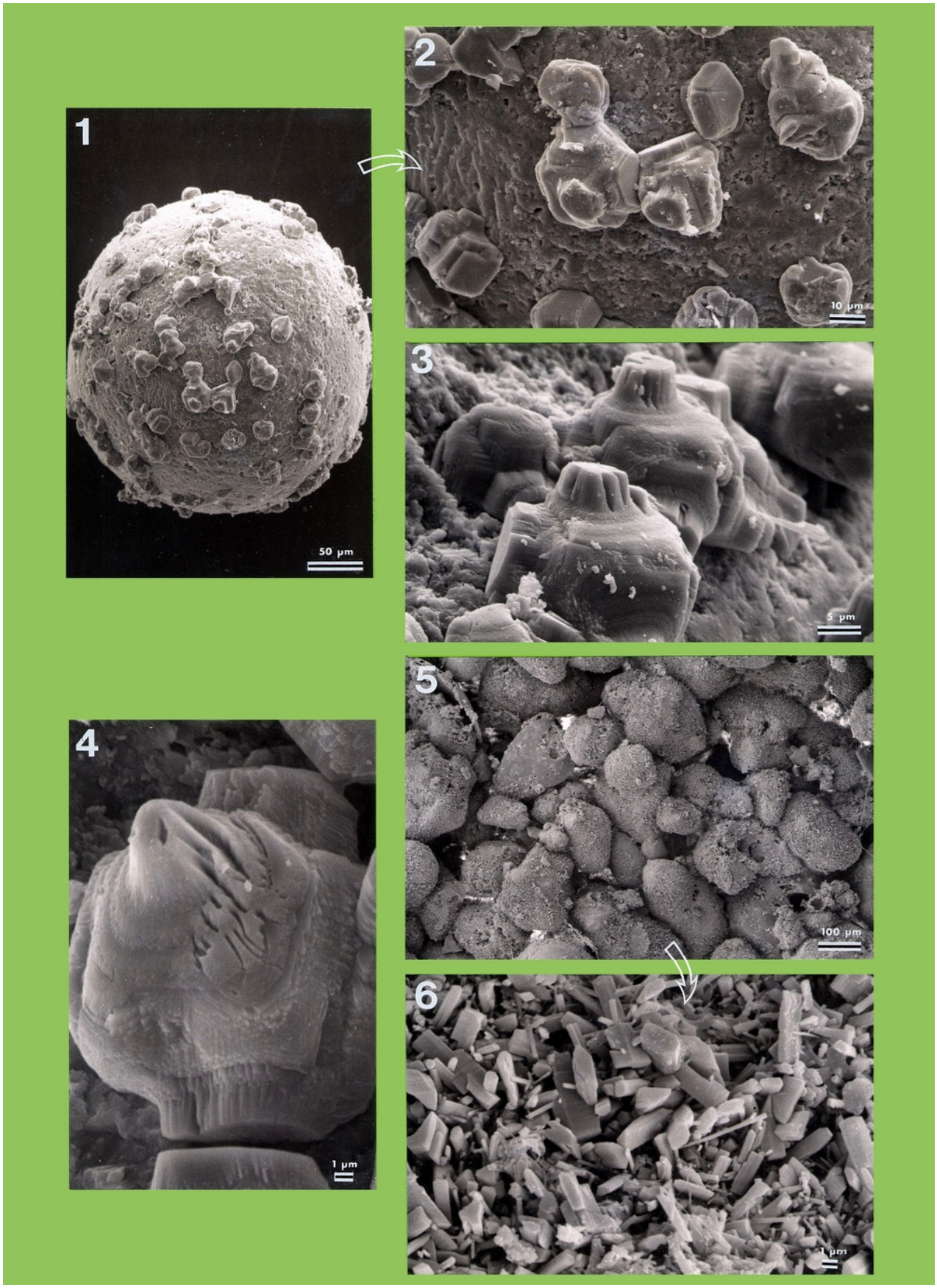
1
50 µm
2
10 µm
3
5 µm
4
1 µm
5
100 µm
6
1 µm

Plate 16: Gypsum

Fig. 1: Lower microbial mat sandwiched between the Pleistocene aeolian sands below and the Holocene lithified Potamid sands above. 0.8 km;
Fig. 2: Microforaminifer embedded in a gypsum poecilitic crystal. Sample ABA 175, 4.2 km - J;
Fig. 3: Random sections of lenticular gypsum crystals. Sample ABA 105, 14E (circa 5.2 km) - II;
Fig. 4: Polygonal sections of gypsum crystals partly converted into anhydrite. Sample ABA 147, 4.2 km - D;
Fig. 5: Felted anhydrite with more or less discernible (arrows) polygonal patterns indicative of replacement of a gypsum precursor. Sample ABA 147, 4.2 km - D.

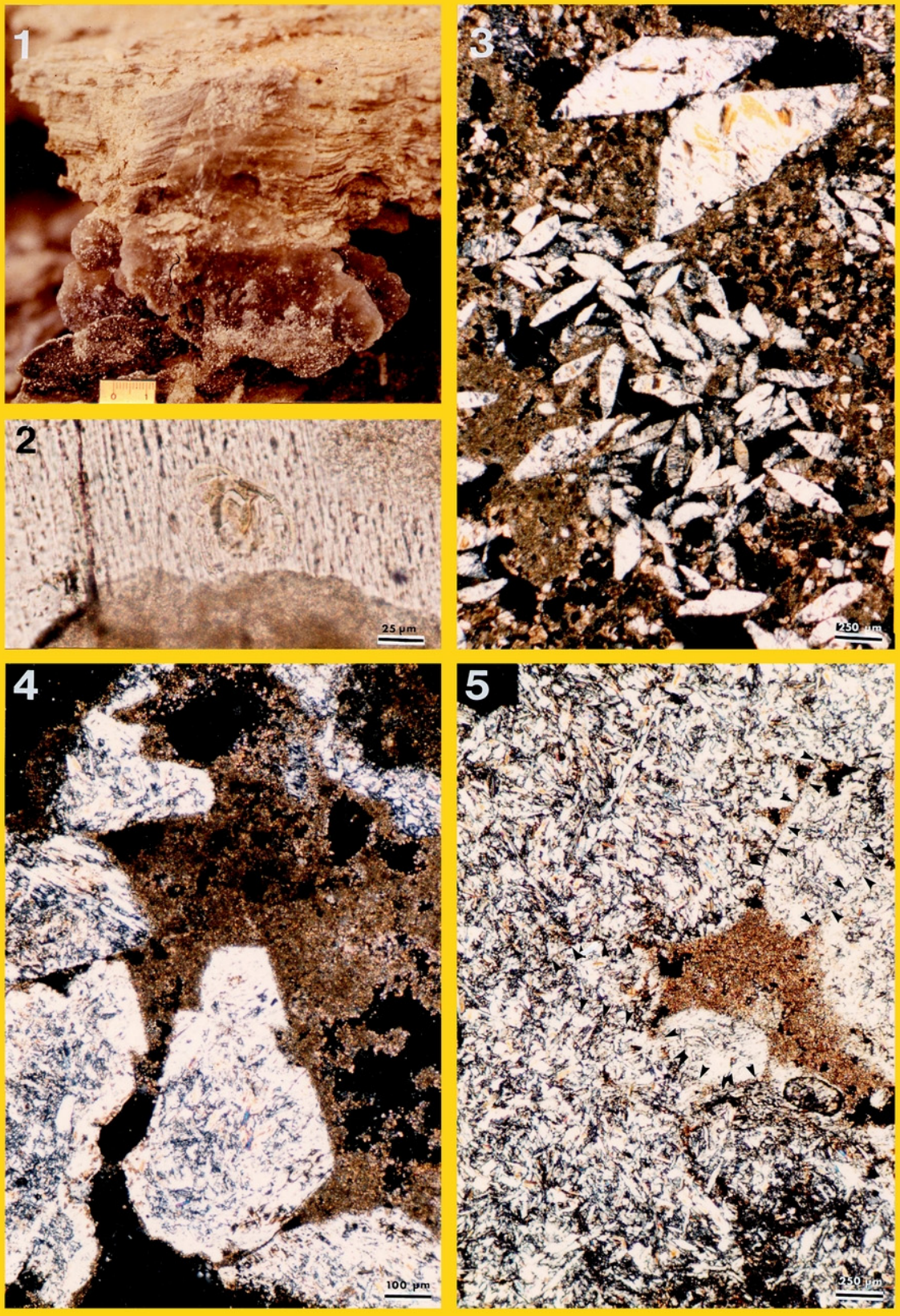
1
2
25 µm
3
250 µm
4
100 µm
5
250 µm

Poster 1: Mussafah channel transect

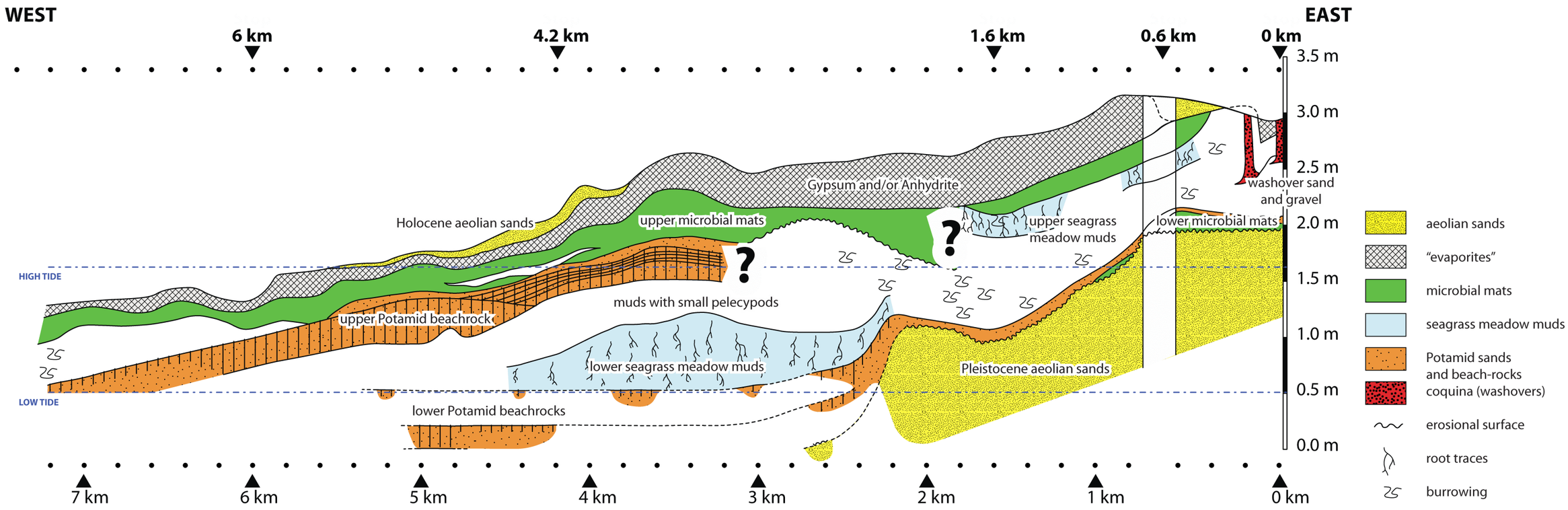

Poster 2: - 2 km (February 1987)

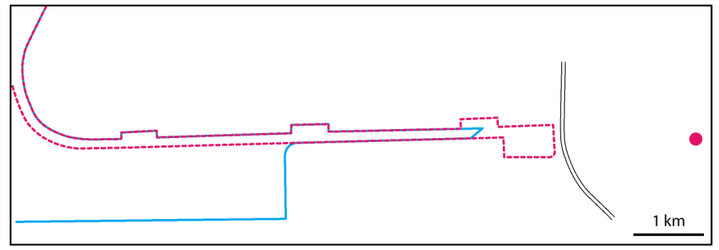

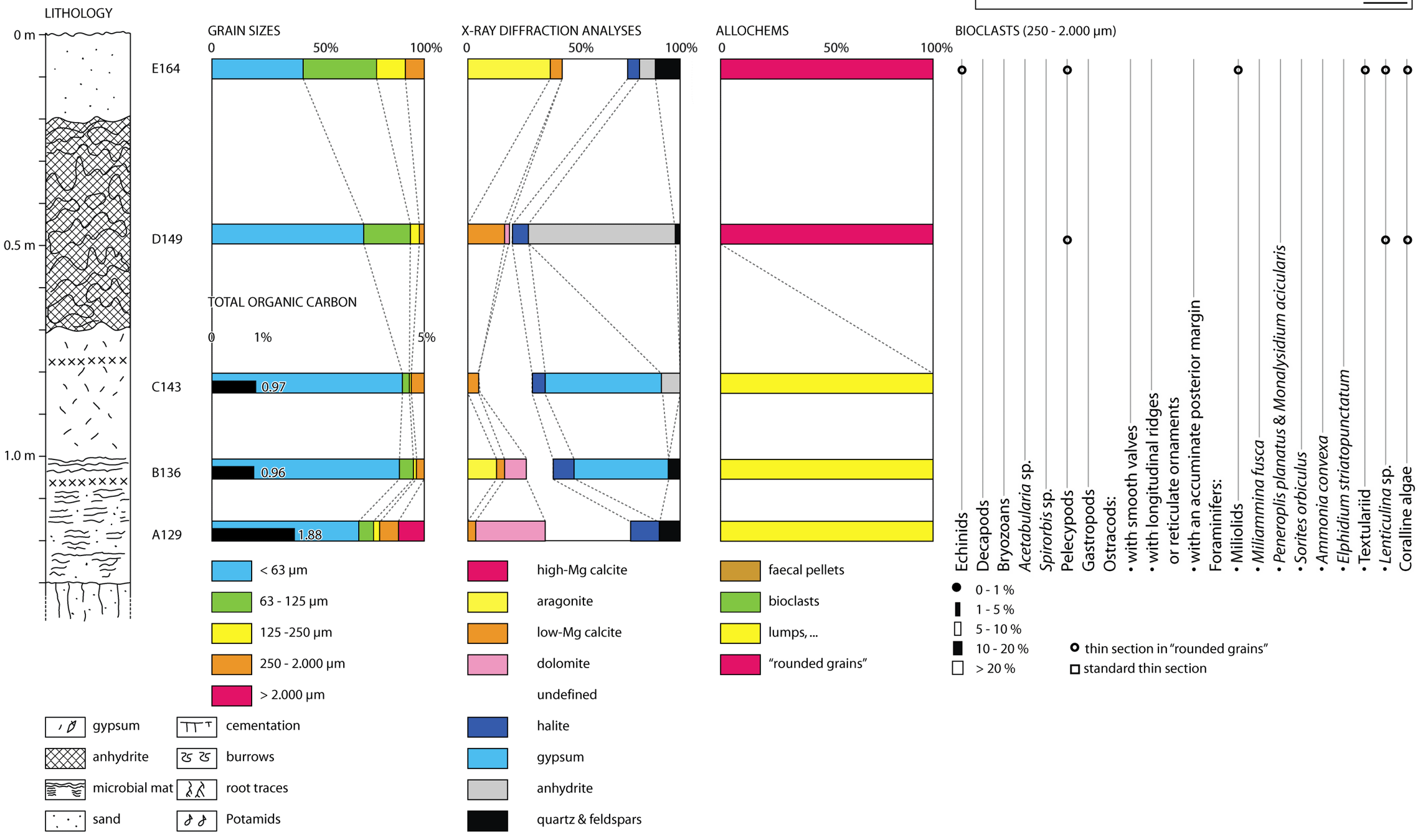

Poster 3: Site14D (April 1986)

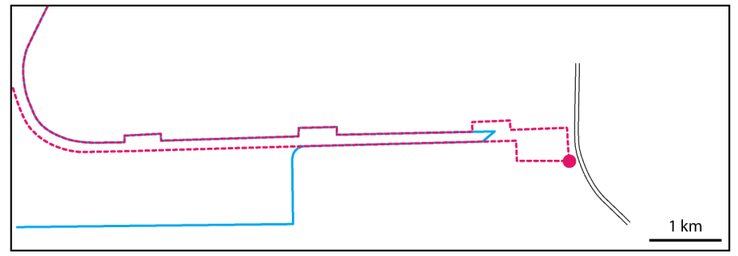

Poster 4: 0 km (February 1987)

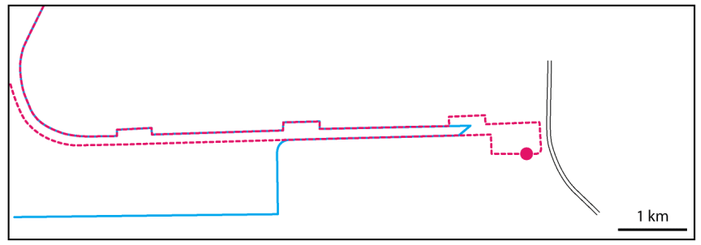

Poster 5: Site 14B (April 1986)

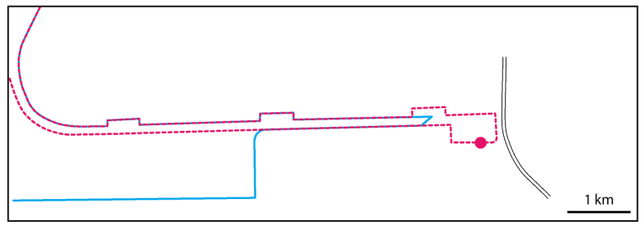

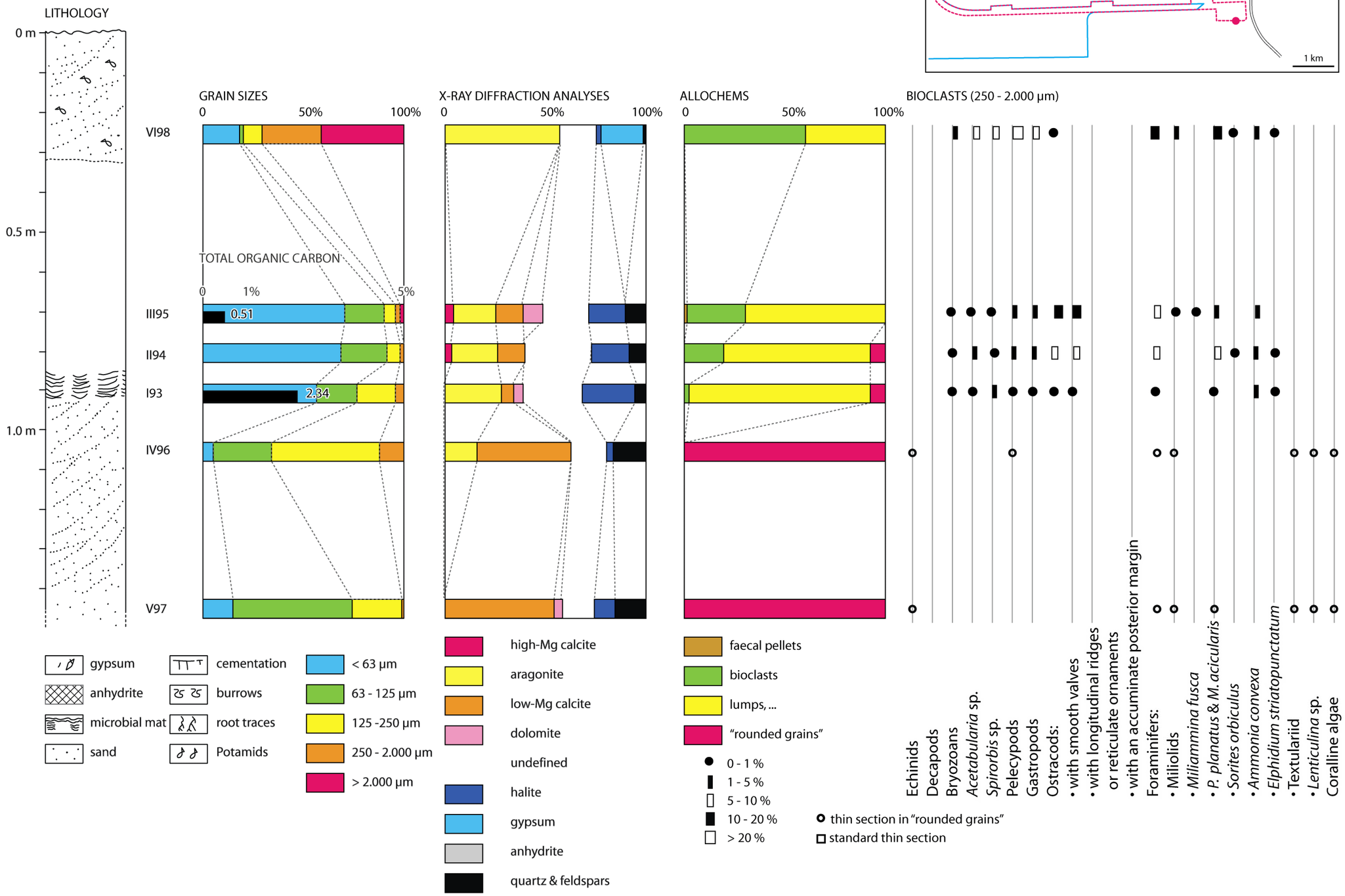

Poster 6: 0.6 km (February 1987)

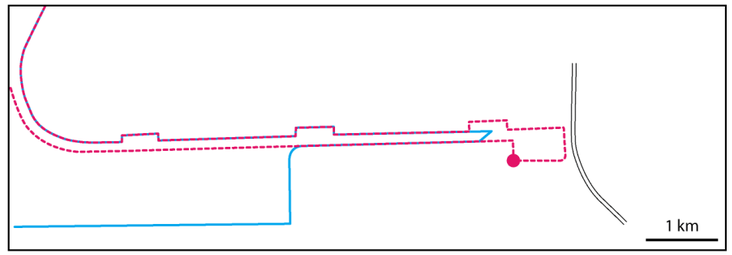

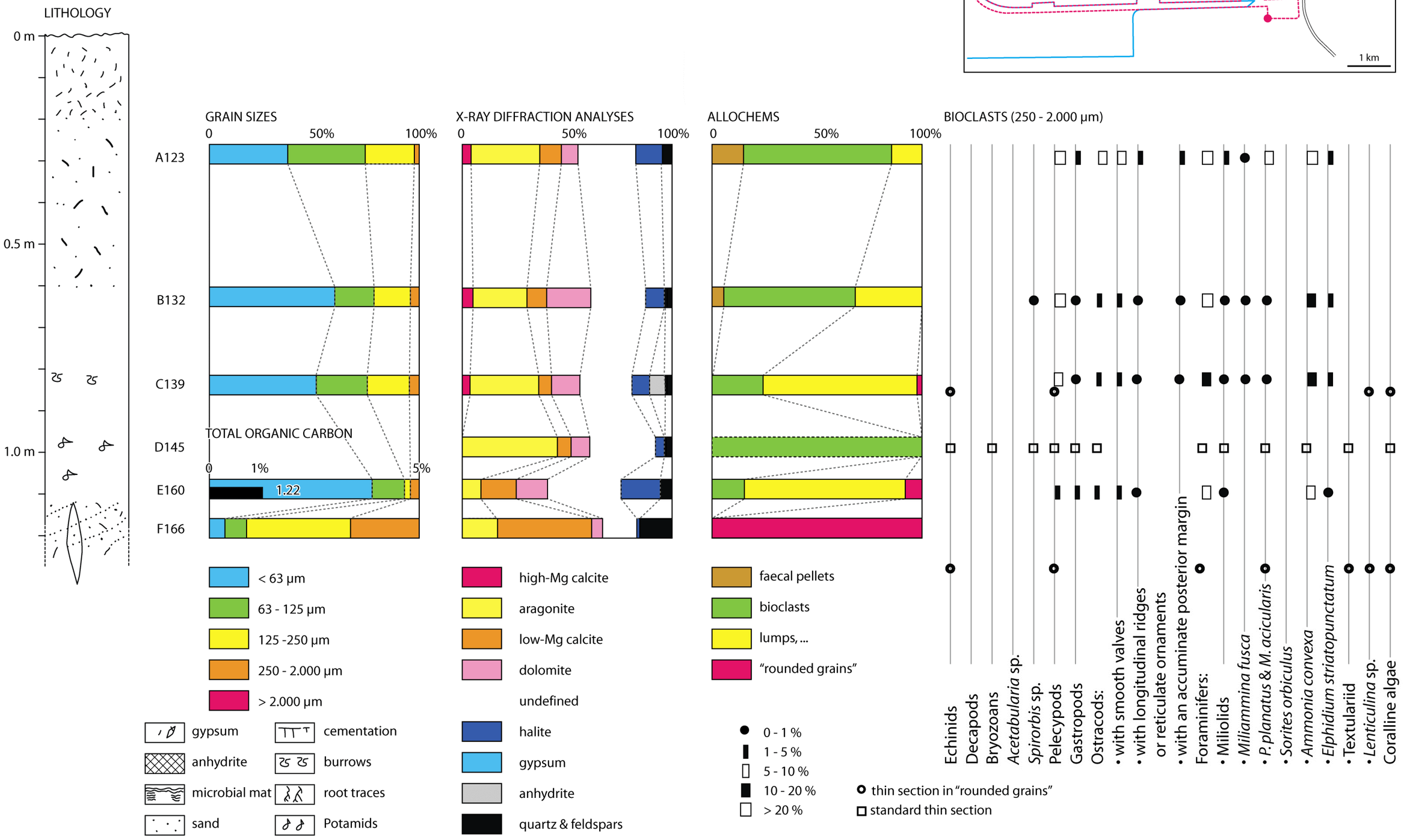

Poster 7: 1.6 km (February 1987)

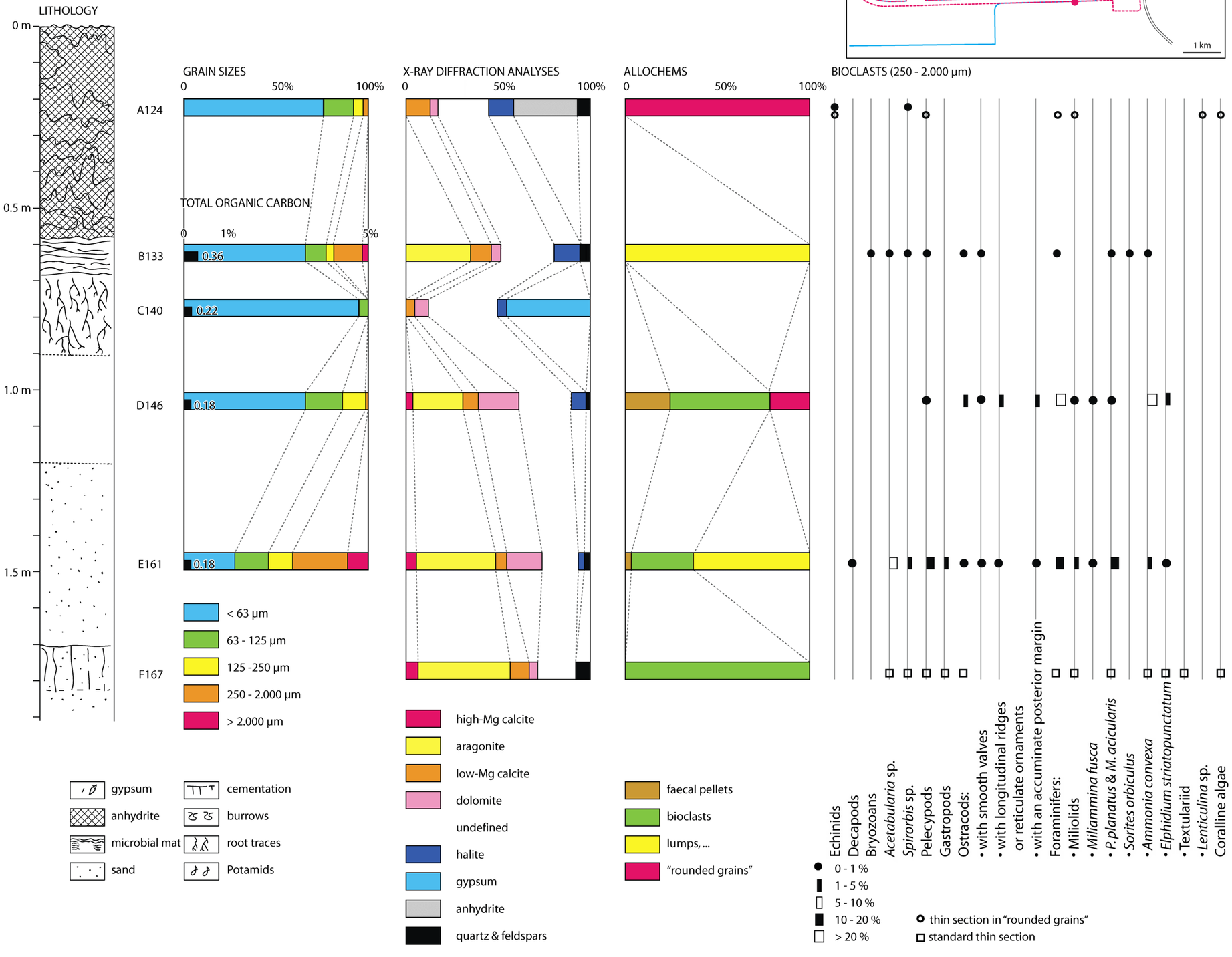

Poster 8: 4.2 km (February 1987)

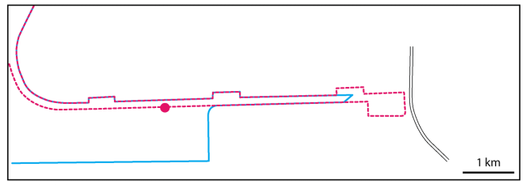

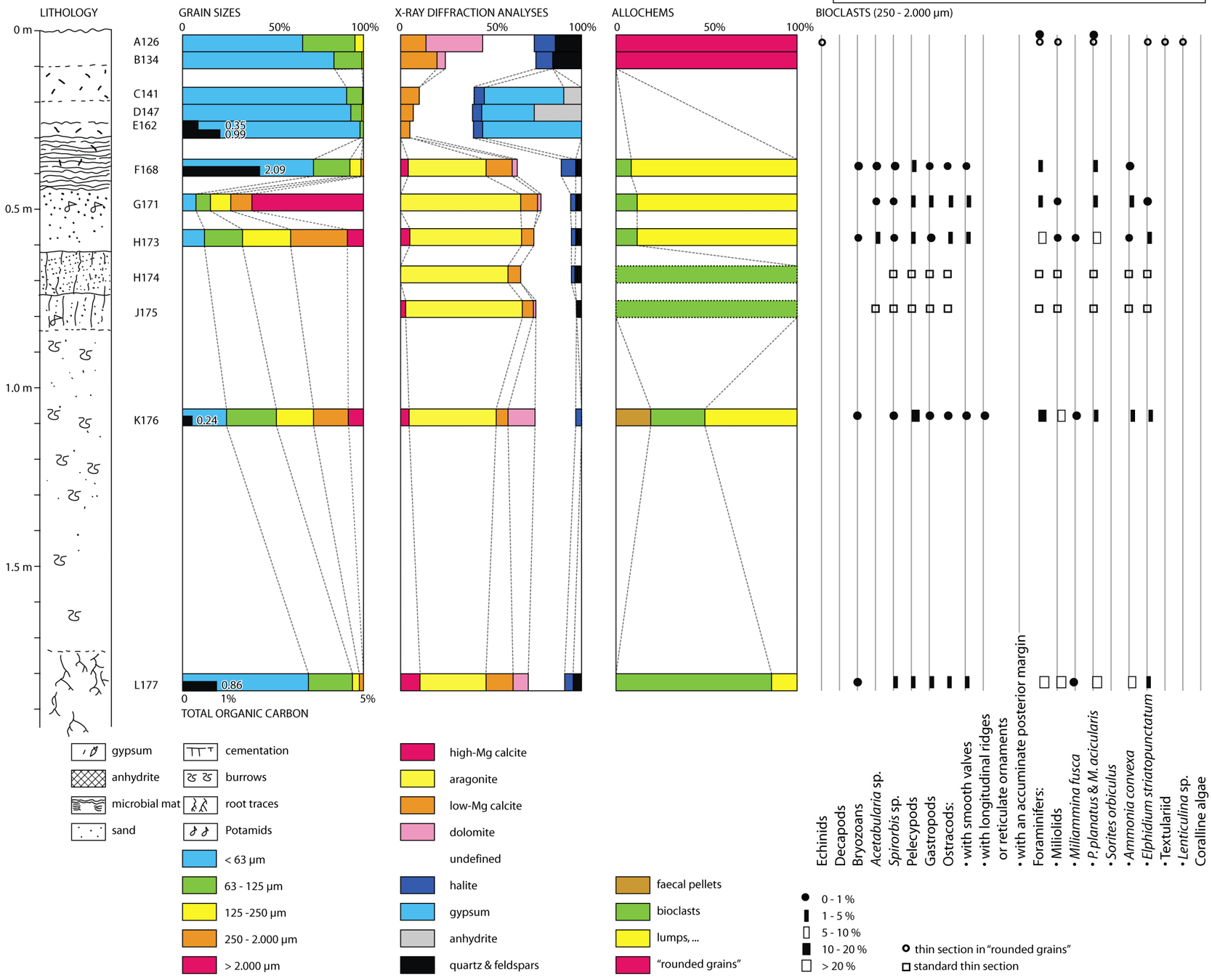

Poster 9: 6 km (February 1987)

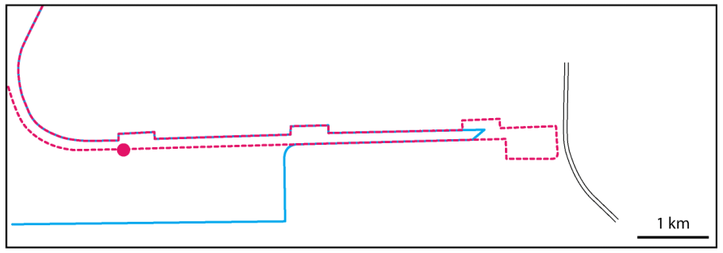

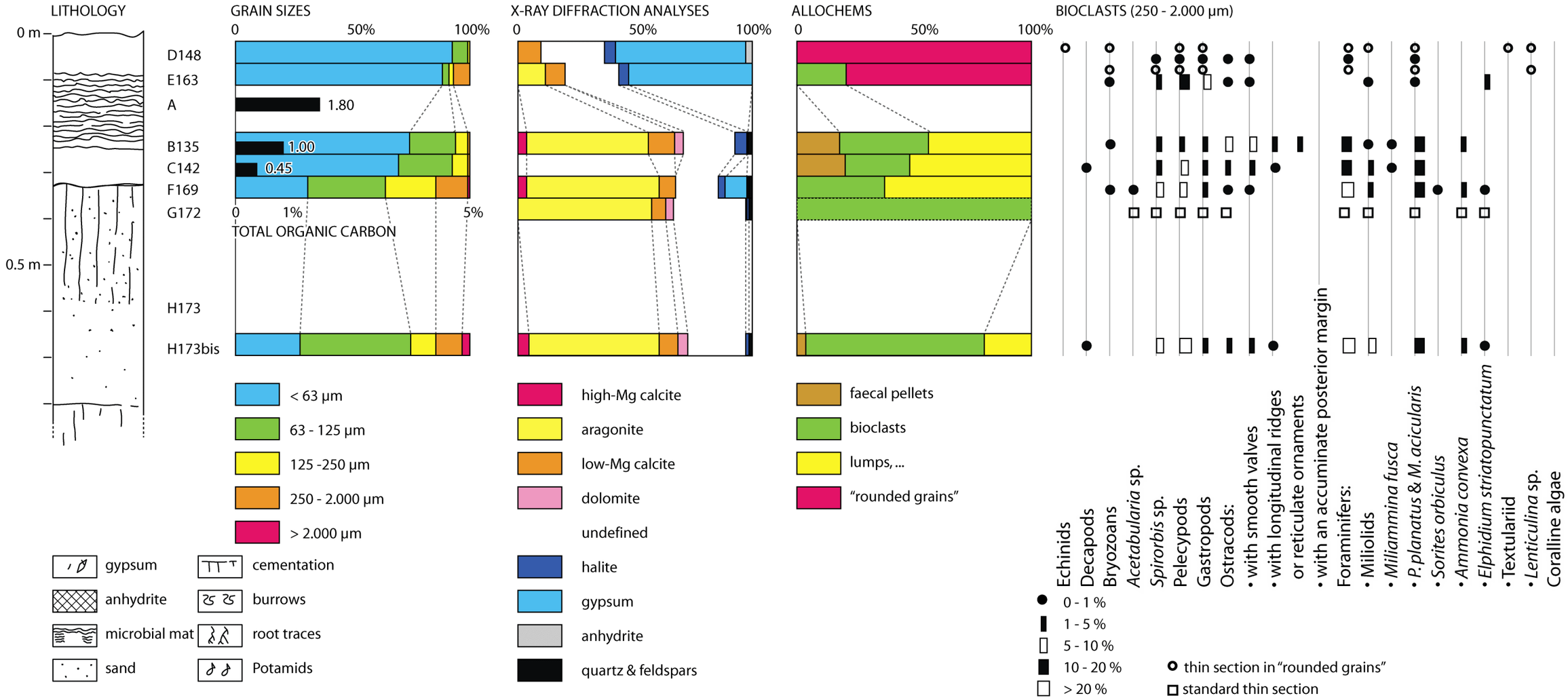

Poster 10: Grain sizes